Radiation of cell suspension

To investigate the validity of bioluminescent monitoring of the effect of ionizing radiation, we irradiated the suspension of Ba/F3-Luc/Wt cells in vitro and evaluated the time course of bioluminescent signals in relation to viable cell numbers. In vitro measurements were performed on days 0, 2, 3, 5, 7, 9, and 11. Immediately after day-2 measurements, the cell suspension was irradiated with 5 Gy using a ^{137}Cs source (Gammacell 1000 Elite; MDS Nordion, Kanata, Ontario, Canada) at a dose rate of 6.4 Gy/min. The culture medium was changed after each set of measurements, and the cell suspension was diluted so that the culture density remained below 3.5×10^5 cell/mL. The viable cell number and luminescence in a given volume of cell suspension were corrected for dilution ratios and expressed as a percentage of day-0 values.

In vivo BLI

In vivo BLI was performed using a cooled charge coupled device camera system (IVIS Imaging System 100; Xenogen, Alameda, CA, USA). Mice received an intraperitoneal injection of 150 mg/kg D-luciferin and were placed in the light-tight chamber of the camera system under isoflurane anesthesia. Beginning 5 minutes after injection, photographic and luminescent images in the dorsal, left-lateral, ventral, and right-lateral projections were acquired. The data acquisition series of four projections was repeated twice; consequently, a single imaging session provided eight luminescent images. Luminescent images were taken with an exposure time of 1 to 60 seconds, binning of 4 or 8, and a field-of-view of 25 cm. Up to five mice were imaged simultaneously.

Monitoring after sublethal TBI

Mice inoculated with Ba/F3-Luc/Wt cells underwent sublethal TBI, and the therapeutic effects were monitored using in vivo BLI longitudinally. In vivo BLI was performed 5 days after cell inoculation, and mice were divided into four groups ($n = 5$ each), one control group and three TBI groups, which had comparable whole-body signals 5 days postinoculation. Seven days after inoculation, the mice underwent in vivo BLI and were then irradiated with various single radiation doses. TBI was performed using a 150-kV x-ray source (MBR-1520R-3; Hitachi, Tokyo, Japan) operating at 20 mA and filtered with 1 mm Al at a rate of 1.81 Gy/min. The three TBI groups were given doses of 3, 4, or 5 Gy, and the control group was sham irradiated. In vivo BLI was performed 8, 10, and 14 days after cell inoculation (1, 3, and 7 days after TBI) and then twice a week until spontaneous death.

Monitoring after lethal TBI

Mice inoculated with Ba/F3-Luc/Wt cells underwent lethal TBI with or without BMT, and were examined by in vivo BLI longitudinally. In vivo BLI was performed before and 5 days after cell inoculation, and mice were divided into two groups ($n = 5$ each), the TBI alone group and the TBI + BMT group, which had comparable whole-body signals 5 days postinoculation. Seven days after inoculation, the mice underwent in vivo BLI and thereafter TBI of 7 Gy. This dose was shown to be above the LD100/30 in preliminary experiments. The BMT was performed for the TBI + BMT group 24 hours after TBI. Bone marrow cells harvested from the femurs and tibias of syngeneic mice (2×10^7 cells in 0.2 mL PBS) were injected via the tail vein. In vivo BLI was performed 10 and 14 days after the inoculation of Ba/F3-Luc/Wt cells (3 and 7 days after TBI) and then twice a week up to 63 days after inoculation. After the day-63 study, only one mouse showing slowly increasing BLI signals remained alive, and BLI was performed once a week until the spontaneous death of the mouse.

Data analysis

To assess whole-body tumor burden from in vivo BLI, a region of interest (ROI) encompassing the entire mouse except the tail and distal ends of the limbs was placed on each in vivo BLI image, and the total signal in the ROI (photons/s) was quantified using the Living Image software (version 2.50; Xenogen). The total signals of all eight images obtained in a single imaging session were averaged to determine the whole-body signal, which was used as a marker of whole-body tumor burden. The 14/7-day signal ratio was determined as the ratio of the whole-body signal 14 days after cell inoculation (7 days after TBI) to that 7 days after inoculation (just before TBI). To assess whole-body tumor burden at spontaneous death, the day of spontaneous death was recorded based on a daily check of survival, and presumptive whole-body signal at death was calculated by extrapolating from the final two data points monoexponentially.

In the study of sublethal TBI, comparisons between groups were made by one-way analysis of variance followed by post-hoc analysis using Fisher's least significant difference tests. Survival was compared with the whole-body signal by linear regression analysis. Statistical testing was conducted after logarithmic transformation of bioluminescence signals and signal ratios. A p value < 0.05 was considered statistically significant.

Results

Radiation of cell suspension

We irradiated Ba/F3-Luc/Wt cells in vitro and evaluated the relationship between cell proliferation and temporal changes in luminescence. Viable cell counting showed depression of cell proliferation 1 day after irradiation and regrowth 7 days after irradiation (Fig. 1A). Viability (Fig. 1C) and proliferation index (Fig. 1D) declined 3 days and 1 day after irradiation, respectively. Both standard and intact-cell luciferase assays demonstrated radiation-induced inhibition of the increase in luminescent signals from a given amount of cell suspension, consistent with depression of cell proliferation (Fig. 1A). However, luminescent signals definitely increased 1 day after irradiation despite minimal augmentation in viable cell number, and correspondingly, luminescence per cell increased (Fig. 1B). The discrepancy between luminescence and viable cell number diminished gradually, and luciferase assays faithfully demonstrated regrowth.

Monitoring after sublethal TBI

Mice received sublethal TBI (3, 4, or 5 Gy) 7 days after intravenous inoculation of Ba/F3-Luc/Wt cells, and in vivo BLI was repeated until spontaneous death. Twenty mice,

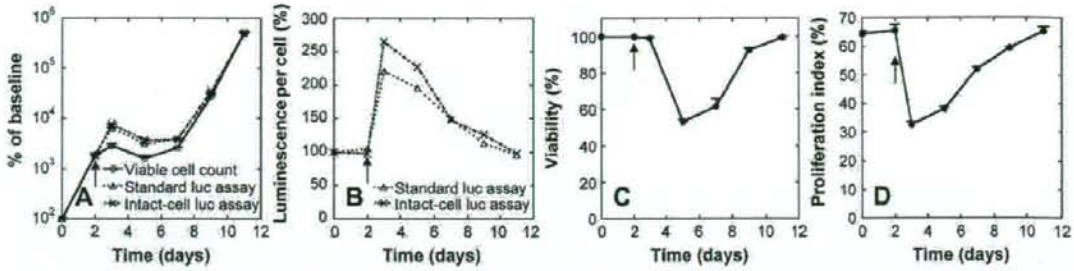

Figure 1. Irradiation of cultured Ba/F3-Luc/Wt cells. The viable cell number, and luminescent signals from the standard luciferase assay and the intact-cell luciferase assay, expressed as percentages of baseline values, increased before irradiation, and the increase was inhibited after irradiation performed on day 2 (**A**). The inhibition was delayed for luminescence, and luminescence per cell increased transiently after irradiation (**B**). Viability (**C**) and proliferation index (**D**) decreased early after irradiation. Arrows indicate the day of irradiation, and error bars represent standard deviations (n = 3).

including nonirradiated control mice, were studied 8 to 12 times, and 189 BLI studies in total were performed, regarding a series of image acquisitions as consisting of five BLI studies when five mice were imaged simultaneously. Unexpectedly, essentially no signals were detected in five studies, suggesting bowel injection of D-luciferin [9,28]. In such cases, D-luciferin was injected again, resulting in reasonable luminescence, and the signals obtained after the second injection were used for analysis.

In vivo BLI demonstrated focal luminescent signals indicative of tumor cell proliferation before TBI (Fig. 2). Control mice showed consistent increases in whole-body signals over time and died 27 to 29 days after cell inoculation (Fig. 3). Bone marrow signals appeared to be dominant early after inoculation, and signals in the spleen and liver became conspicuous later. TBI caused transient inhibition of increase in whole-body signals and prolonged survival in a dose-dependent manner. Signals increased 1 day after TBI, similar to the control group, and decreased thereafter. Regrowth tended to be delayed after greater radiation doses. Spontaneous death occurred at similar signal levels, regardless of radiation dose. The presumptive whole-body signal at death had a relatively narrow range, from 6.70×10^9 to 2.16×10^{10} photons/s, for all 20 mice and did not differ significantly among groups.

A significant negative correlation was found between survival and whole-body signals 14 days after inoculation, 7 days after TBI (Fig. 4; $r = -0.8000$, $p < 0.0001$). Survival differed significantly among groups (Fig. 5A; $p < 0.01$) and tended to be longer in mice receiving greater doses although it was marginally shorter in the 4-Gy group than in the 3-Gy group. In the post-hoc analysis, significant differences were demonstrated between controls and the 3-Gy group, between controls and the 5-Gy group, and between the 4-Gy and 5-Gy groups, but not between controls and the 4-Gy group, between the 3-Gy and 4-Gy groups, or between the 3-Gy and 5-Gy groups. The 14/7-d signal ratio, indicating signal increase during 7 days after TBI, differed significantly among groups (Fig. 5B; $p < 0.0001$) and was smaller in mice receiving greater doses. Dose dependence was more evident for the 14/7-d signal ratio than for survival, and the post hoc analysis of the 14/7-d signal ratio vs dose showed significant differences for all pairs.

Monitoring after lethal TBI

Mice underwent lethal TBI (7 Gy) with or without BMT and were followed by repeated in vivo BLI. In total, 118 BLI studies were performed and additional D-luciferin injection was required in four studies because of apparent injection failure.

Lethal TBI caused profound reduction in whole-body signals (Fig. 6), although residual disease was demonstrated even at maximal reduction by both visual evaluation and quantitative analysis of the BLI images. Mice in the TBI alone group died 20 to 22 days after cell inoculation while whole-body signals remained weak, consistent with treatment-related death. In the TBI + BMT group, in vivo BLI showed minimal signals 17 days after inoculation (10 days after TBI), followed by regrowth. The 14/7-d signal ratio ranged from 0.12 to 0.30, and the maximum value was smaller than the minimum value in the sublethal TBI groups. Survival was largely prolonged in this group. Four mice died 48 to 63 days after cell inoculation, and presumptive whole-body signals at death were similar to those in the experiments of sublethal TBI (7.17×10^9 - 2.15×10^{10} photons/s). The other mouse showed a slow increase in whole-body signals and survived much longer (97 days). Despite the marked difference in survival time, the mouse did not differ substantially in presumptive whole-body signals at death from those of other mice (6.51×10^9 photons/s).

Discussion

We investigated the application of in vivo BLI in assessing the effect of TBI in an animal model of a hematological malignancy. First, we evaluated the time course of viable cell numbers and bioluminescence signals after irradiation

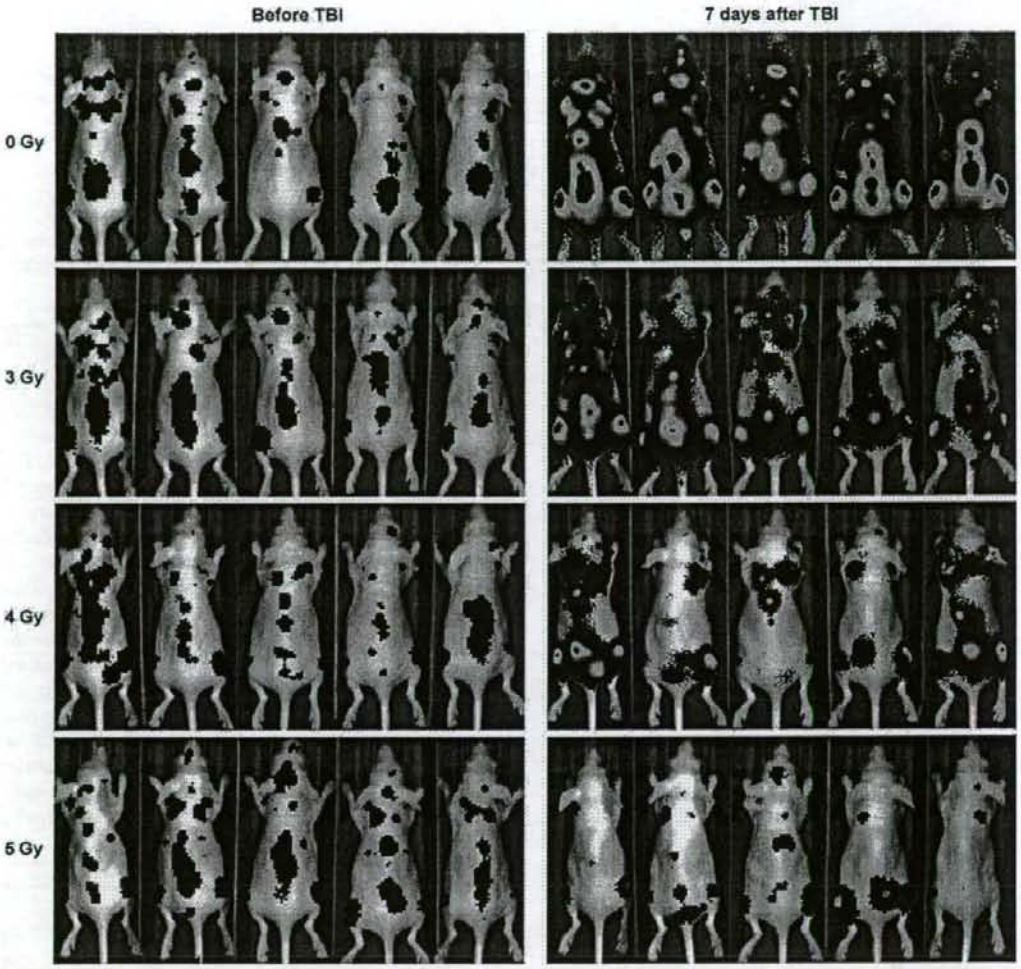

Figure 2. Dorsal images of in vivo bioluminescence imaging acquired before and 7 days after sublethal total body irradiation (TBI) (7 and 14 days after cell inoculation). The pseudocolor luminescent image (blue, green, yellow, and red from least to most intense) is overlaid on the grayscale photographic image. The same color scale was used for all panels. Dose-dependent inhibition of disease progression is shown.

of cell suspension to evaluate the validity of bioluminescent signals in tumor monitoring after radiotherapy. Irradiation inhibited cell proliferation transiently, as expected. Luciferase assays demonstrated the inhibitory effect and regrowth similar to viable cell counting, supporting the use of bioluminescence signals as an index of viable tumor burden after irradiation. However, luminescence per cell increased immediately after irradiation, which could cause an overestimation of viable tumor burden in BLI tumor monitoring. It has been reported that ionizing radiation transcriptionally activates the LTRs of Moloney murine sarcoma virus [29], Rous sarcoma virus [30], and human immunodeficiency virus type 1 [31], although it does not influence the activity of the cytomegalovirus immediate-early promoter or the simian virus 40 promoter [30]. In the cells studied in this study, luciferase was expressed under the control of the MMLV LTR, and our observations indicated transcriptional activation of the MMLV LTR by irradiation. Whereas we previously demonstrated that the addition of imatinib to the suspension of Ba/F3-Luc/Wt cells decreases both proliferation index and luminescence per cell [25], increase in luminescence per cell was associated with decrease in proliferation index in the present study. The change in the activity of MMLV LTR cannot be explained by dependence on cell cycle. Ionizing radiation activates various signal transduction pathways [32,33] and many transcription

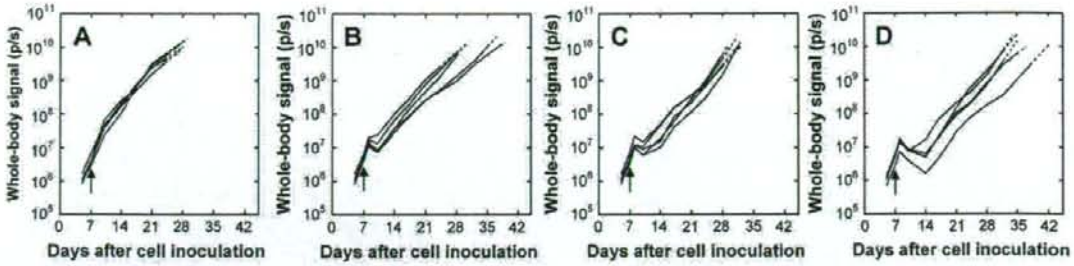

Figure 3. Time courses of whole-body bioluminescence signals in each mouse of the control group (**A**) and three sublethal total body irradiation (TBI) groups (**B**, 3 Gy; **C**, 4 Gy; **D**, 5 Gy). TBI was performed 7 days after cell inoculation (arrows). The solid lines were drawn between the measured points, and the broken lines were drawn by extrapolation to the day of spontaneous death.

factors can bind to the enhancer region of MMLV LTR [34,35]. Although the molecular mechanism of the activation of MMLV LTR remains to be elucidated, the results of our cell culture study indicate that luminescence signals from luciferase-expressing cells would approximate viable tumor burden but the relationship may be distorted to some extent early after irradiation.

In mice of a hematological malignancy model, sublethal TBI caused transient inhibition of increase in whole-body signals and prolonged survival in a dose-dependent manner. Although whole-body signals increased on the day after TBI, the increase may not imply increase in tumor burden. Bioluminescence signals immediately after irradiation may have overestimated viable cell numbers due to the activation of the MMLV LTR in vivo as well as in vitro. Whole-body signals 7 days after TBI correlated with survival, indicating the potential of in vivo BLI signals as an early surrogate marker for assessing therapeutic response. In vivo BLI appears to allow early prediction of therapeutic efficacy and may contribute to improving the efficiency of experiments. Moreover, although significant dose dependence was demonstrated for both survival and signal increase during 7 days after TBI, the dependence was more evident for signal increase. Generally, a clearer dose-response relationship can be expected for radiotherapy than for drug therapy due to consistency of delivery and lack of metabolic interference. The rate of tumor regrowth after early response, pretreatment tumor burden, and tumor burden causing death have interindividual variation independent of treatment protocol, which may to some extent obscure the relationship between radiation dose and survival. The clearer dose–response relationship for signal increase suggests that in vivo BLI enables the evaluation of antitumor effects more precisely than survival assessment and that statistically significant results can be obtained more readily in comparing the effects of different treatments. In addition, presumptive whole-body signals at death showed small interindividual differences when compared to the wide signal range observed during the entire course and were independent of radiation dose, supporting the concept that BLI signals reflect disease severity even after treatment.

In mice receiving lethal TBI followed by syngeneic BMT, prolongation of survival and reduction in BLI signals were prominent, suggesting that higher doses can offer better outcomes. Residual signals were demonstrated even at maximal responses, and regrowth was monitored longitudinally. Presumptive whole-body signals at death were similar to those in nonirradiated or sublethally irradiated mice, suggesting that tumor burden causing spontaneous death was not influenced largely by the treatment. Mice that underwent lethal TBI not followed by BMT died while showing weak BLI signals, indicating that death was not due to progression of malignancy but due to the adverse effects of the treatment. Although the dose was known to be lethal and treatment-related death was predictable in the present study, nontumor-related death may occur unexpectedly from treatment-related

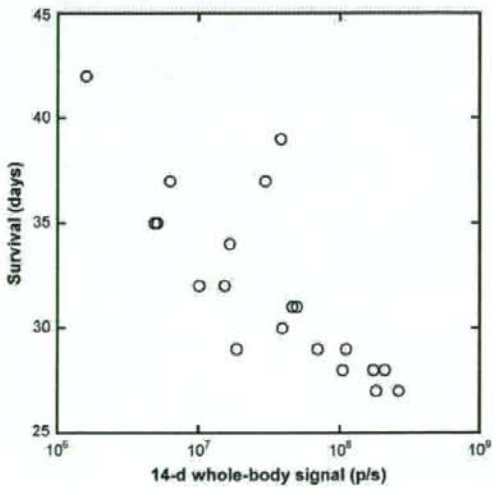

Figure 4. Relationship of survival with whole-body signals 14 days after inoculation (7 days after sublethal total body irradiation). A significant negative correlation was demonstrated ($r = -0.8000$, $p < 0.0001$).

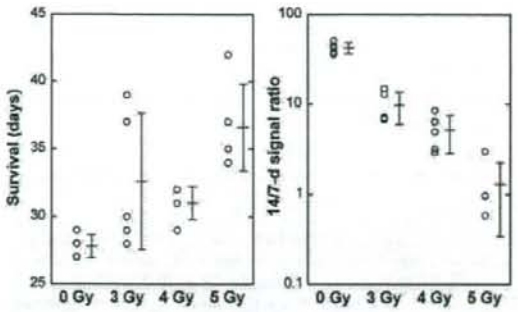

Figure 5. Survival (left) and 14/7-day signal ratio (right) in mice receiving various doses of sublethal total body irradiation (TBI). Plots indicate data for individual mice. Mean and standard deviations are also presented. Dose dependence is more evident for the 14/7-day signal ratio, an index of signal increase during 7 days after TBI, than for survival.

damage or incidentally and should be discriminated from death by tumor progression. In vivo BLI allows the evaluation of tumor burden independently of survival and appears to aid the discrimination between tumor-related and nontumor-related deaths and the assessment of antitumor effects in mice that died from nontumor-related causes.

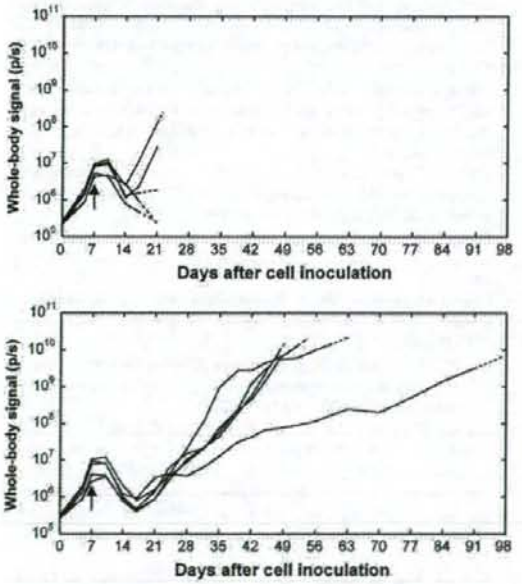

Figure 6. Time courses of whole-body bioluminescence signals in each mouse of the total body irradiation (TBI) alone group (upper) and TBI + bone marrow transplantation group (lower). Lethal TBI (7 Gy) was performed 7 days after cell inoculation (arrows). Solid lines were drawn between the measured points, and the broken lines were drawn by extrapolation to the day of spontaneous death. Whole-body signals before cell inoculation, which were not measured in experiments of sublethal TBI, were plotted as day-0 values.

The relationship between in vivo BLI signals and tumor burden may be distorted by various factors. Quantitative estimates of bioluminescence depend on luciferase expression per viable cell, delivery of D-luciferin to luciferase-expressing cells, availability of cofactors (oxygen, adenosine triphosphate, and magnesium) for the luminescent reaction, scattering and absorption of light photons in the tissues, and the determination of ROIs. Our results support bioluminescent evaluation of tumor burden and therapeutic responses in the model used, despite the possible influence of confounding factors. However, substantial signals were not acquired after the first intraperitoneal administration of D-luciferin in nine of 307 BLI studies (2.9%), which appeared to be attributable to bowel injection [9,28] and exemplifies problems with D-luciferin delivery. The possibility of alterations in luciferase activity per viable cell induced by therapeutic intervention was also highlighted, as indicated previously using the MMLV LTR [25] and the cytomegalovirus immediate-early promoter [36,37]. Although the utility of in vivo BLI monitoring of therapeutic efficacy would hold true not only for TBI but also other treatment modalities, it should be noted that luminescence per viable cell may vary early after therapy depending on the type of therapeutic intervention and the promoter driving luciferase expression, resulting in a discrepancy between viable tumor burden and BLI signals. Due to the rapid progression of the disease model used in the present study, only minor differences in survival could be observed. Further evaluation using less aggressive models would be desired.

Our study demonstrates that in vivo BLI allows longitudinal, quantitative evaluation of the response to TBI in a murine hematological malignancy model. Whole-body BLI signals reflect whole-body tumor burden even after TBI with or without BMT, and the antitumor effect can be assessed early, reliably, and independently of survival. Signal change early after treatment, as an alternative to survival, can be used as a marker of therapeutic response for efficient testing of various treatment protocols, and nontumor-related deaths can be determined based on weak BLI signals. Our study also illustrates the need for considering the influence of the treatment on promoter activity, in addition to the general utility of in vivo BLI.

Acknowledgments

This study was supported in part by Grants-in-Aid for Scientific Research from the Ministry of Education, Culture, Sports, Science and Technology of Japan.

References

1. Contag CH, Jenkins D, Contag PR, Negrin RS. Use of reporter genes for optical measurements of neoplastic disease in vivo. Neoplasia. 2000;2:41–52.

2. Edinger M, Cao YA, Hornig YS, et al. Advancing animal models of neoplasia through in vivo bioluminescence imaging. Eur J Cancer. 2002;38:2128–2136.
3. Inoue Y, Izawa K, Tojo A, et al. Monitoring of disease progression by bioluminescence imaging and magnetic resonance imaging in an animal model of hematologic malignancy. Exp Hematol. 2007;35: 407–415.
4. Edinger M, Cao YA, Verneris MR, Bachmann MH, Contag CH, Negrin RS. Revealing lymphoma growth and the efficacy of immune cell therapies using in vivo bioluminescence imaging. Blood. 2003; 101:640–648.
5. Shah NP, Tran C, Lee FY, Chen P, Norris D, Sawyers CL. Overriding imatinib resistance with a novel ABL kinase inhibitor. Science. 2004; 305:399–401.
6. Wu KD, Cho YS, Katz J, et al. Investigation of antitumor effects of synthetic epothilone analogs in human myeloma models in vitro and in vivo. Proc Natl Acad Sci U S A. 2005;102:10640–10645.
7. Armstrong SA, Kung AL, Mabon ME, et al. Inhibition of FLT3 in MLL. Validation of a therapeutic target identified by gene expression based classification. Cancer Cell. 2003;3:173–183.
8. Xin X, Abrams TJ, Hollenbach PW, et al. CHIR-258 is efficacious in a newly developed fibroblast growth factor receptor 3-expressing orthotopic multiple myeloma model in mice. Clin Cancer Res. 2006; 12:4908–4915.
9. Paroo Z, Bollinger RA, Braasch DA, et al. Validating bioluminescence imaging as a high-throughput, quantitative modality for assessing tumor burden. Mol Imaging. 2004;3:117–124.
10. Nogawa M, Yuasa T, Kimura S, et al. Monitoring luciferase-labeled cancer cell growth and metastasis in different in vivo models. Cancer Lett. 2005;217:243–253.
11. Szentirmai O, Baker CH, Lin N, et al. Noninvasive bioluminescence imaging of luciferase expressing intracranial U87 xenografts: correlation with magnetic resonance imaging determined tumor volume and longitudinal use in assessing tumor growth and antiangiogenic treatment effect. Neurosurgery. 2006;58:365–372.
12. Smakman N, Martens A, Kranenburg O, Borel Rinkes IH. Validation of bioluminescence imaging of colorectal liver metastases in the mouse. J Surg Res. 2004;122:225–230.
13. Mandl SJ, Mari C, Edinger M, et al. Multi-modality imaging identifies key times for annexin V imaging as an early predictor of therapeutic outcome. Mol Imaging. 2004;3:1–8.
14. Jenkins DE, Oei Y, Hornig YS, et al. Bioluminescent imaging (BLI) to improve and refine traditional murine models of tumor growth and metastasis. Clin Exp Metastasis. 2003;20:733–744.
15. Scatena CD, Hepner MA, Oei YA, et al. Imaging of bioluminescent LNCaP-luc-M6 tumors: a new animal model for the study of metastatic human prostate cancer. Prostate. 2004;15(59):292–303.
16. Zeamari S, Rumping G, Floot B, Lyons S, Stewart FA. In vivo bioluminescence imaging of locally disseminated colon carcinoma in rats. Br J Cancer. 2004;90:1259–1264.
17. Nyati MK, Symon Z, Kievit E, et al. The potential of 5-fluorocytosine/ cytosine deaminase enzyme prodrug gene therapy in an intrahepatic colon cancer model. Gene Ther. 2002;9:844–849.
18. Rehemtulla A, Stegman LD, Cardozo SJ, et al. Rapid and quantitative assessment of cancer treatment response using in vivo bioluminescence imaging. Neoplasia. 2000;2:491–495.
19. Wissink EH, Verbrugge I, Vink SR, et al. TRAIL enhances efficacy of radiotherapy in a p53 mutant, Bcl-2 overexpressing lymphoid malignancy. Radiother Oncol. 2006;80:214–222.
20. Lee CK. Evolving role of radiation therapy for hematologic malignancies. Hematol Oncol Clin North Am. 2006;20:471–503.
21. Kal HB, Loes van Kempen-Harteveld M, Heijenbrok-Kal MH, Struikmans H. Biologically effective dose in total-body irradiation and hematopoietic stem cell transplantation. Strahlenther Onkol. 2006; 182:672–679.
22. Gabriel DA, Shea TC, Serody JS, et al. Cytoprotection by amifostine during autologous stem cell transplantation for advanced refractory hematologic malignancies. Biol Blood Marrow Transplant. 2005;11: 1022–1030.
23. Nieder C, Licht T, Andratschke N, Peschel C, Molls M. Influence of differing radiotherapy strategies on treatment results in diffuse large-cell lymphoma: a review. Cancer Treat Rev. 2003;29:11–19.
24. Gustavsson A, Osterman B, Cavallin-Ståhl E. A systematic overview of radiation therapy effects in non-Hodgkin's lymphoma. Acta Oncol. 2003;42:605–619.
25. Inoue Y, Tojo A, Sekine R, et al. In vitro validation of bioluminescent monitoring of disease progression and therapeutic response in leukaemia model animals. Eur J Nucl Med Mol Imaging. 2006;33:557–565.
26. Copelan EA, McGuire EA. The biology and treatment of acute lymphoblastic leukemia in adults. Blood. 1995;85:1151–1168.
27. Li S, Ilaria RL Jr, Million RP, Daley GQ, Van Etten RA. The P190, P210, and P230 forms of the BCR/ABL oncogene induce a similar chronic myeloid leukemia-like syndrome in mice but have different lymphoid leukemogenic activity. J Exp Med. 1999;189:1399–1412.
28. Baba S, Cho SY, Ye Z, Cheng L, Engles JM, Wahl RL. How reproducible is bioluminescent imaging of tumor cell growth? Single time point versus the dynamic measurement approach. Mol Imaging. 2007;6: 315–322.
29. Lin CS, Goldthwait DA, Samols D. Induction of transcription from the long terminal repeat of Moloney murine sarcoma provirus by UV-irradiation, x-irradiation, and phorbol ester. Proc Natl Acad Sci U S A. 1990;87:36–40.
30. Cheng X, Iliakis G. Effect of ionizing radiation on the expression of chloramphenicol acetyltransferase gene under the control of commonly used constitutive or inducible promoters. Int J Radiat Biol. 1995;67:261–267.
31. Faure E, Cavard C, Zider A, Guillet JP, Resbeut M, Champion S. X irradiation-induced transcription from the HIV type 1 long terminal repeat. AIDS Res Hum Retroviruses. 1995;11:41–43.
32. Dent P, Yacoub A, Contessa J. Stress and radiation-induced activation of multiple intracellular signaling pathways. Radiat Res. 2003;159: 283–300.
33. Chastel C, Jiricny J, Jaussi R. Activation of stress-responsive promoters by ionizing radiation for deployment in targeted gene therapy. DNA Repair. 2004;3:201–215.
34. Kim S, Lee K, Kim MD, et al. Factors affecting the performance of different long terminal repeats in the retroviral vector. Biochem Biophys Res Commun. 2006;343:1017–1022.
35. LoSardo JE, Cupelli LA, Short MK, Berman JW, Lenz J. Differences in activities of murine retroviral long terminal repeats in cytotoxic T lymphocytes and T-lymphoma cells. J Virol. 1989;63:1087–1094.
36. Svensson RU, Barnes JM, Rokhlin OW. Chemotherapeutic agents upregulate the cytomegalovirus promoter: implications for bioluminescence imaging of tumor response to therapy. Cancer Res. 2007;67: 10445–10454.
37. Kim KI, Kang JH, Chung JK, et al. Doxorubicin enhances the expression of transgene under control of the CMV promoter in anaplastic thyroid carcinoma cells. J Nucl Med. 2007;48:1553–1561.

Leukemia (2008) 22, 1131–1138

www.nature.com/leu

ORIGINAL ARTICLE

RNAi-mediated silencing of p190$^{Bcr-Abl}$ inactivates Stat5 and cooperates with imatinib mesylate and 17-allylamino-17-demetoxygeldanamycin in selective killing of p190$^{Bcr-Abl}$-expressing leukemia cells

M Futami[1], T Hatano[2], Y Soda[1], S Kobayashi[1], M Miyagishi[3] and A Tojo[1]

[1]*Division of Molecular Therapy, Advanced Clinical Research Center, Institute of Medical Science, University of Tokyo, Tokyo, Japan;* [2]*Department of Chemistry and Biotechnology, School of Engineering, University of Tokyo, Tokyo, Japan and* [3]*The 21st Century Center of Excellence (COE) Program, Graduate School of Medicine, University of Tokyo, Tokyo, Japan*

The 190 kD (p190) and 210 kD (p210) Bcr-Abl proteins are responsible for the pathophysiology of Philadelphia chromosome (Ph)$^+$ leukemia. We applied RNA interference (RNAi) to specific killing of p190$^+$ cells, and determined the optimal sequences for gene silencing in the BCR, junctional and ABL regions of p190, respectively. Then, p190$^+$ and p210$^+$ cells were infected with lentiviral vectors encoding these shRNAs, resulting in efficient killing of p190$^+$ cells, while p210$^+$ cells were only sensitive to shBCR and shABL. In p190-transformed Ba/F3 cells, silencing of p190 specifically inhibited tyrosine phospohorylation of Stat5 prior to their death, but did not affect phosphorylation of Jak2, Akt or MEK1/2. In contrast, downregulation of p190 by their treatment with 17-allylamino-17-demetoxygeldanamycin (17-AAG) was associated with reduced protein levels of Jak2, Akt and MEK1/2. shRNA targeting p190 collaborated additively with imatinib and 17-AAG in growth inhibition of Ba/F3-p190wt and imatinib-resistant Ba/F3-p190Y253H cells. Collectively, RNAi-mediated silencing of p190 is a promising option both for delineating signal transduction and for therapeutic application in 190$^+$ leukemia.
Leukemia (2008) **22**, 1131–1138; doi:10.1038/leu.2008.60; published online 27 March 2008
Keywords: Bcr-Abl; Ph$^+$ALL; RNAi; lentiviral vector; 17-AAG; Stat5

Introduction

Philadelphia chromosome (Ph)$^+$ leukemia, including chronic myeloid leukemia (CML) and acute lymphoblastic leukemia (Ph$^+$ALL), originates from hematopoietic stem/progenitor cells affected by the BCR-ABL fusion gene, which encodes constitutively active tyrosine kinase essential for development and progression of the diseases.[1] There are two major forms of Bcr-Abl protein, p210 and p190. The former is associated with almost all cases of CML and less than half of Ph$^+$ALL cases, whereas the latter mainly causes Ph$^+$ALL except for very rare cases of CML.[2]

The development of imatinib (also referred to as STI571), and the second generation tyrosine kinase inhibitors have greatly improved the clinical outcome of CML.[3–5] However, Ph$^+$ALL shows a much less durable response to these kinase inhibitors, and easily acquires resistance, caused primarily by point mutations in the Abl kinase domain such as T315I.[6,7] To overcome the resistance, the downregulation of Bcr-Abl proteins is a promising strategy for eliminating Ph$^+$ALL cells, irrespective of point mutations. From this viewpoint, we have previously reported that lentiviral delivery of anti-p190 maxizyme specifically induces apoptosis in Ph$^+$ALL cells.[8]

Recently, RNA interference (RNAi) has been recognized as a more powerful tool in the selective gene silencing. RNAi allows downregulation of target genes at the post-transcriptional level via sequence-specific mRNA depletion. This can be accomplished by the delivery of double-strand RNA in the form of small interfering RNA (siRNA) or small hairpin RNA (shRNA).[9,10] Anti-p210 RNAi targeting sequences of the junctional domain of Bcr-Abl suppressed its expression in CML cell lines, resulting in growth inhibition,[11,12] and lentivirus-mediated stable expression of anti-p210 shRNA has also been successful.[13,14] Similarly, electroporation of p190$^+$ cells with anti-p190 siRNA downregulated p190 and reduced cell viability in a dose-dependent fashion.[15] However, this procedure may exert nonspecific toxicity on intact cells, and short-lived siRNA is not suitable for monitoring cell viability. Therefore, to precisely evaluate the consequences of RNAi-mediated p190 silencing, viral vector-mediated transfer and stable expression of shRNA in p190$^+$ cells are required.

In the present study, we successfully downregulated p190 by lentiviral transduction with shRNA targeting p190, resulting in efficiently killing of p190$^+$ cells. We also observed that silencing of p190 caused specific inactivation of Stat5 and cooperated with imatinib and 17-allylamino-17-demetoxygeldanamycin (17-AAG) in the selective killing of p190$^+$ cells.

Materials and methods

Design of shRNAs targeting p190

Three types of 21-bp shRNA were designed, and named as shE1A2, shABL and shBCR, respectively. shE1A2 targets junctional lesion between BCR exon 1 and ABL exon 2 (e1a2) in p190 mRNA. The sequence was determined after the screening by a transient transfection of 293/p190 cells with a series of U6-promoter driven shE1A2 expression vectors, in which we found that the center of junctional lesion was suitable for target site (Supplementary Figure 1). We also designed shABL targeting nt 1238–1258 of ABL, and shBCR targeting nt 992-1012 of BCR, with a computer algorithm (iGENE Therapeutics, Tsukuba, Japan) to identify optimal sequences, and tested for their ability to downregulate p190 (Supplementary Figure 2). shLUC targeting *Renilla* luciferase was prepared as a control. Although shE1A2 is supposed to be specific for p190, shABL is

Correspondence: Dr A Tojo, Division of Molecular Therapy, Advanced Clinical Research Center, Institute of Medical Science, University of Tokyo, 4-6-1 Shirokanedai, Munato-ku, Tokyo 108-8639, Japan.
E-mail: a-tojo@ims.u-tokyo.ac.jp
Received 26 August 2007; revised 18 February 2008; accepted 19 February 2008; published online 27 March 2008

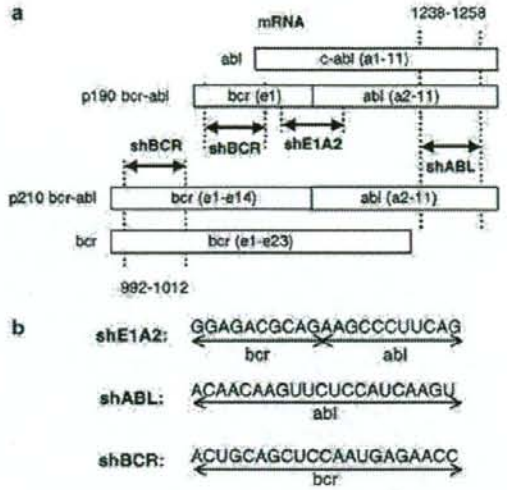

Figure 1 Target sites for shRNAs. (**a**) Locations of target site. Arrows indicate the target sites of shRNAs on abl, e1a2 of p190 Bcr-Abl, e14a2 of p210 Bcr-Abl and bcr mRNA. (**b**) The target site sequences. Arrows indicate areas in which the sequence is complementary to that of bcr or abl.

predicted to affect not only p190 but also p210 and Abl. Similarly, shBCR is predicted to affect p190, p210 as well as Bcr (Figures 1a and b).

Production of lentiviral vectors

The nucleotide sequences of the shRNA expression cassette in the piGENE-PURhU6/shRNA were amplified by polymerase chain reaction using Platinum *pfx* DNA polymerase (Invitrogen, Carlsbad, CA, USA) and a primer set containing a *Bam*HI site (forward 5′-ATGGATCCAAGGTCGGGCAGGAAGAGG-3′ and reverse 5′-ATGGATCCCATGATGATTACGCCAAGCTTGCAT-3′). The resulting fragments were digested with *Bam*HI and ligated into a *Bam*HI-digested self-inactivating lentiviral transfer vector. The expression cassettes for shE1A2, shABL and shLUC were inserted into lentiviral transfer vector pCS-CDF-EG-PRE containing elongation factor 1α (EF1α) promoter-driven human CD2 as a selection marker (pHIV-CD2), and the shBCR expression cassette was inserted into a similar transfer vector containing CD271 as a marker (pHIV-CD271). Lentiviral vector particles were produced by cotransfection of 293T cells with pHIV-hU6/shRNA, pMDLg/p.RRE, pRSV-rev and pMD.G as described previously.[16] Transduction efficiency was analyzed by flow cytometry of marker gene expression, resulting in 94–99% at high multiplicity of infection (MOI = 5) and around 50% (36–59%) at low MOI (MOI = 1).

Western blot analysis

Cells were lysed, and 50 μg of the lysate were electrophoresed in SDS-polyacrylamide gels, transferred onto polyvinylidene fluoride membranes, and blotted with the respective antibodies, according to the manufactures' instructions. All secondary antibodies were peroxidase-conjugated, and proteins were detected using enhanced chemiluminescence (Amersham, Arlington Heights, IL, USA). The following antibodies were

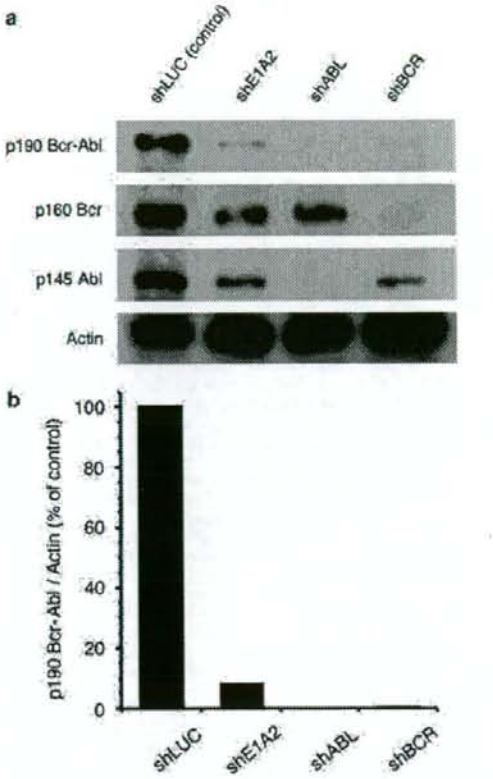

Figure 2 Lentivirus-mediated RNAi silences the expression of p190 Bcr-Abl. (**a**) HEK 293/p190 cells were transduced with shLUC (control), shE1A2, shABL and shBCR at an MOI of 5. The cells were lysed on day 3, and lysates were labeled with the respective antibodies: p190 Bcr-Abl and p145 Abl, with anti-Abl antibody; p160 Bcr, with anti-Bcr antibody and and actin, with anti-actin antibody. The transduction efficiencies, determined by FACS analysis of marker gene expression on day 3: shLUC, 99.1%; shE1A2, 99.3%; shABL, 96.9% and shBCR, 98.1%. (**b**) Quantitative analysis of p190 expression. Quantitative analysis was performed using NIH Image 1.63 (National Institutes of Health, Bethesda, MD, USA), and p190 levels were normalized by actin.

used: anti-Abl (8E9; BD Biosciences, San Diego, CA, USA), anti-Bcr (N-20; Santa Cruz Biotechnology, Santa Cruz, CA, USA), anti-Jak2 (06-255; Upstate Biotechnology, Lake Placid, NY, USA), anti-phospho-Jak2 (Tyr1007/1008; Upstate Biotechnology), and anti-Stat5 (C-17; Santa Cruz Biotechnology); anti-phospho-Stat5 (Tyr694), anti-Akt1, (2H10), anti-phospho-Akt (Ser473), anti-MEK1/2 (L38C12), anti-phospho-MEK1/2 (Ser221) (all from Cell Signaling Technology, Danvers, MA, USA); anti-Actin (AC-40; Sigma, St Louis, MO, USA), sheep anti-mouse IgG (515-036-072; Jacson ImmunoResearch Labolatories, West Grove, PA, USA) and donkey anti-rabbit IgG (NA934V; Amersham Biosciences, Little Chalfont, Bucks, UK).

Cell count and viability assay

Aliquots of 5×10^4 cells (10^5 cells for KOPN-30 cells) in 1 ml of culture medium were plated in a 24-multiwell plate. Cell

number and viability were determined by trypan blue dye exclusion. For cell proliferation assay, 10^3 cells in 100 µl of culture medium were grown in a 96-multiwell plate. Viable cell number was assessed on day 4 using WST-8 assay kit (Seikagaku, Tokyo, Japan).

Colony-forming assay

Human CD34$^+$ cells were purified from umbilical cord blood mononuclear cells by a two-round separation procedure using the Indirect CD34 MicroBead Kit (Miltenyi Biotec, Auburn, CA, USA). Purified CD34$^+$ cells were cultured in α-minimal essential medium containing 30% fetal bovine serum (FBS), 50 ng ml^{-1} hSCF, 50 ng ml^{-1} hTPO, 10 ng ml^{-1} hIL-3 and 50 ng ml^{-1} Flt3L for 24 h, transduced with anti-p190 shRNA lentiviral vectors at an MOI of 20, and incubated for 48 h. Aliquots of 10^3 transduced cells were plated in triplicate in 1 ml of 0.9% methylcellulose containing 30% FBS, 50 ng ml^{-1} hSCF, 10 ng ml^{-1} hIL-3, 100 ng ml^{-1} hG-CSF, and 2 U ml^{-1} hEPO. After 14 days, the number of each type of colony was scored.

Results

Silencing effect of anti-p190 shRNA lentiviral vectors

To confirm the silencing effect, we transduced HEK 293/p190 cells with lentiviral vectors encoding anti-p190 shRNA (shE1A2, shABL and shBCR) at an MOI of 5, and the expression level of p190 was determined by western blot analysis. p190 Bcr-Abl expression were substantially suppressed (0.0–8.0%) by these three anti-p190 shRNAs (Figures 2a and b). The expression of p145 Abl and p160 Bcr was substantially inhibited by shABL and shBCR, respectively (Figure 2a).

Proliferation and survival of leukemia cell lines after the transduction of shRNAs

To investigate the biological consequences of anti-p190 shRNAs, p190$^+$ KOPN-30 cells, p210$^+$ K562 cells and p190/p210$^-$ NALM-6 cells were infected with lentiviral vectors encoding these shRNAs at an MOI of 5, and cell proliferation and viability were determined by trypan blue dye exclusion. The Ph$^+$ ALL-derived KOPN-30 p190$^+$ cells ceased proliferation at two days after transduction with shE1A2, shABL and shBCR, and decreased in cell number and viability in a time-dependent manner, confirming that shRNA-mediated downregulation of p190 can kill Ph$^+$ ALL cells (Figure 3). Given that shABL and shBCR would be expected to knock down both p190 and p210, we assessed the effect of these shRNAs in K562 cells, which express p210. As expected, shABL and shBCR eradicated the K562 cells, whereas shE1A2 did not have a notable effect, indicating that shE1A2 is sequence-specific to p190 (Figure 3). To further confirm that RNAi-mediated downregulation is target sequence specific, we also transduced p190/p210$^-$ NALM-6 cells. None of the anti-p190 shRNAs affected survival in NALM-6 cells, although shABL appeared to have some inhibitory effect on growth, which suggests that p145 Abl may be positively involved in NALM-6 cell proliferation.

The effect of shRNAs on imatinib-resistant cells

To determine whether anti-p190 shRNAs overcome imatinib resistance, murine Ba/F3 cells transformed with wild-type p190 or imatinib-resistant mutant (p190Y253H) were transduced with shE1A2, shABL and shBCR. In the absence of IL-3, these shRNAs depleted BaF/3 cells with both types of p190 in an equipotent manner (Figure 4 left). Supplementation of IL-3 clearly rescued these cells from shRNA-mediated cytotoxic effects, suggesting that signal transduction machinery downstream of IL-3 receptor might be maintained irrespective of p190 expression (Figure 4 right).

The effect of downregulation of Abl and Bcr on normal hematopoiesis

We tested the effects of shABL and shBCR on cytokine-dependent clonal growth and differentiation of normal CD34$^+$ cells. Figure 4b shows that shBCR did not influence colony

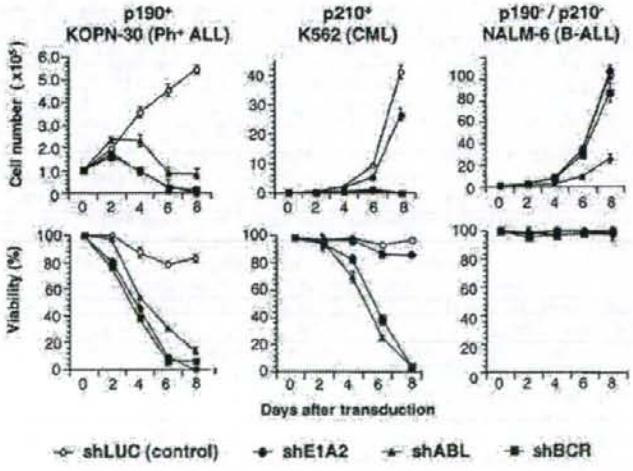

Figure 3 RNAi targeting the junctional domain of p190 kills specifically p190$^+$ cells; RNAi targeting Abl or Bcr kills both p190$^+$ cells and p210$^+$ cells. Cells were transduced with shLUC (control), shE1A2, shABL and shBCR at an MOI of 5. Cell number and viability was determined by the trypan blue exclusion.

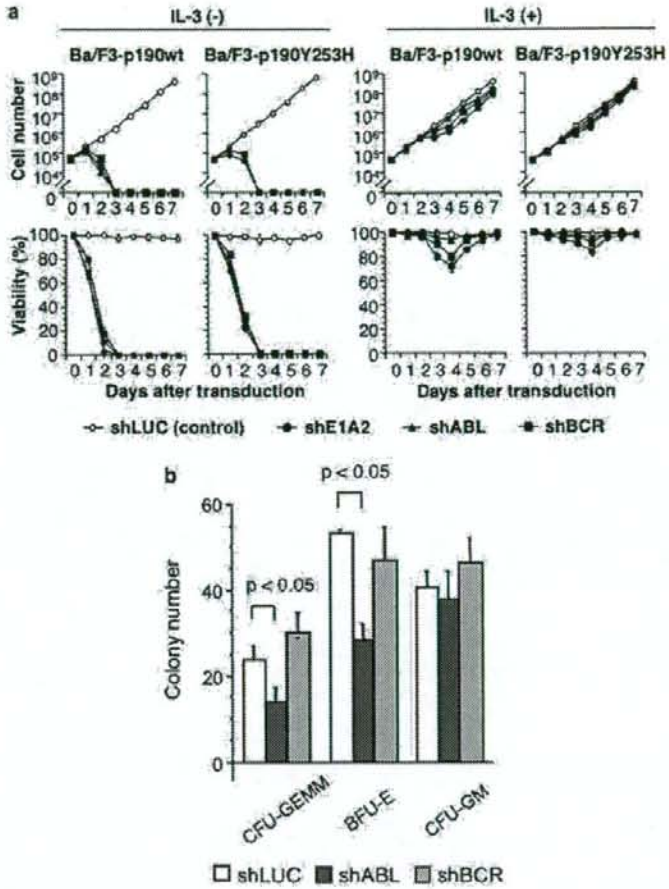

Figure 4 (**a**) Anti-p190 shRNAs kill BaF/3-p190 cells, and supplementation with IL-3 rescues these cells. Cells were transduced with shLUC, shE1A2, shABL and shBCR at an MOI of 5, and cultured in the absence or presence (10 ng ml^{-1}) of murine IL-3. Cell number and viability were determined by trypan blue exclusion. (**b**) Knock-down of Abl suppresses hematopoietic colony formation of normal cord blood CD34$^+$ cells. Cord blood CD34$^+$ cells were transduced with shRNA lentiviral vectors at an MOI of 20, and cytokine-dependent clonal growth was examined by the methylcellulose hematopoietic colony-forming assay. The number of various types of colonies was scored after 14 days in culture.

formation derived from colony-forming unit granulocyte-erythrocyte-monocyte-megakariocyte (CFU-GEMM), CFU granulocyte-monocyte (CFU-GM), and burst-forming unit erythroid (BFU-E) cells, but shABL markedly suppressed CFU-GEMM and BFU-E-derived colony formation.

The effect of Anti-p190 shRNA on p190 and the downstream signal transduction pathway

Bcr-Abl kinase activates a number of signal transduction pathways, including the Jak/Stat, PI3K/Akt and Ras/Raf/MEK/ERK pathways.[17] However, the relative contributions of these signaling pathways to p190-triggered proliferation and survival are not fully understood. To elucidate the primary event that is directly influenced by the downregulation of p190 Bcr-Abl, Ba/F3-p190wt cells were transduced with anti-p190 shRNAs, and the phosphorylation status of molecules involved in Bcr-Abl-mediated transformation was determined by immunoblot analysis at 48 h after transduction (Figure 5a). There were no significant changes in phosphorylation status of Jak2 by the treatment with anti-p190 shRNAs. In contrast, a marked reduction in phosphorylated Stat5 was noted in anti-p190 shRNA-treated BaF/3-p190wt cells, supporting the idea that p190 activates Stat5 in a Jak2-independent manner. Anti-p190 shRNAs did not significantly affect phosphorylation of Akt or MEK1/2. These results imply that downregulation of p190 rapidly results in the inactivation of Stat5, but inactivation of either PI3K/Akt or Ras/Raf/MEK/ERK pathway is not significant compared with Stat5.

The effect of 17-AAG on p190 and the downstream signal transduction pathway

Treatment with 17-AAG disrupts Hsp90 function and degrades its client protein, p190/p210.[18,19] Ba/F3-p190wt cells were treated with increasing concentrations of 17-AAG for 24 h, and

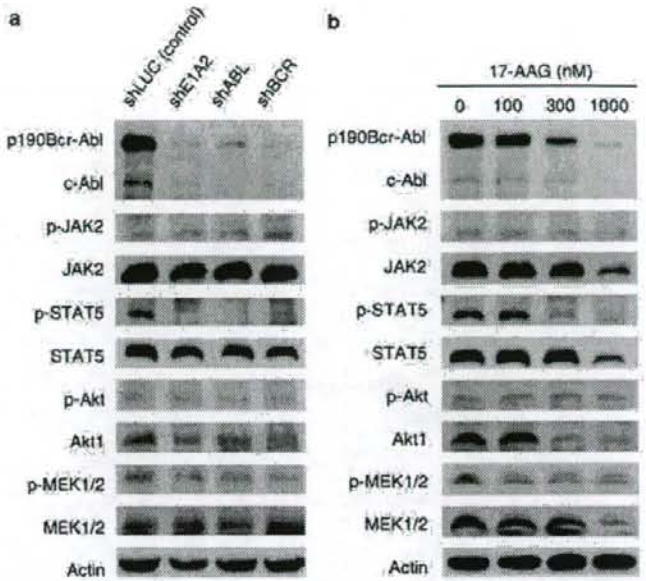

Figure 5 Western blot analysis of Ba/F3-p190wt cells. (**a**) Ba/F3-p190wt cells were transduced with shRNA lentiviral vectors at an MOI of 5. Cells were harvested at 48 h after transduction, lysed and labeled with the respective antibodies. (**b**) Ba/F3-p190wt cells were cultured in the presence or absence of 17-AAG (0–1000 nM) for 24 h. Lysates were labeled with the respective antibodies.

the expression level and phosphorylation status of the same molecules shown in Figure 5a were analyzed. As shown in Figure 5b, 17-AAG downregulated both p190 and p145 Abl in a dose-dependent manner at concentrations >300 nM. The Jak2 protein level was downregulated at 1000 nM. The downregulation of phosphorylated Stat5 preceded that of total Stat5 protein level, which was not affected by the treatment with 17-AAG up to 300 nM. Akt1 and MEK1/2 were downregulated by 17-AAG at around 300 nM. These results suggest that 17-AAG affects p190 as well as various molecules involved in Bcr-Abl-mediated transformation.

Combined effects between shRNA, imatinib and 17-AAG

Because anti-p190 RNAi and 17-AAG can downregulate p190 by different mechanisms, and imatinib inactivates the kinase activity of p190, their combination may work in a synergistic or additive manner in killing of Ba/F3-p190wt and BaF/3-p190Y253H cells. These two cell lines were transduced with anti-p190 shRNAs in a suboptimal condition (MOI = 1) and cultured with increasing dose of either imatinib or 17-AAG. Under these conditions, anti-p190 shRNAs increased sensitivity of Ba/F3-p190wt cells to imatinib and 17-AAG. BaF/3-p190Y253H cells did not respond to imatinib, even at 5 μM; however, the anti-p190 shRNAs appeared to restore sensitivity to higher concentrations of imatinib (Figure 6a). On the other hand, anti-p190 shRNAs cooperated with 17-AAG to kill Ba/F3-p190Y253H cells, with a dose-response curve similar to that in Ba/F3-p190wt cells (Figure 6b). When Ba/F3-p190 cells were exposed to various dosage combinations of 17-AAG and imatinib, the drugs acted synergistically to kill Ba/F3-p190wt cells, and 17-AAG clearly sensitized Ba/F3-p190Y253H cells to imatinib (Figure 6c).

Discussion

We applied RNAi to test whether specific and efficient killing of Ph$^+$ ALL cells could be achieved by downregulation of p190. Wohlbold *et al.*[15] first reported the effective inhibition of p190 protein by siRNA and its cytotoxicity in murine 32D-p190 cells; however, they induced siRNA by elecroporation, which is likely to cause nonspecific damage to recipient cells. We independently designed a series of overlapping shRNAs complementary to the e1a2 junction of p190 and determined the optimal target sequence for inhibition, finding a sequence identical to that described by Wohlbold *et al.* Use of lentiviral transfer of shRNA expression cassettes provided efficient transduction and sustained silencing of the target protein with reduced nonspecific damage. Using a similar vector system, Scherr *et al.*[14] have demonstrated that stable, but not transient, RNAi can efficiently deplete p210 from p210$^+$ cells, depending on the MOI used for infection; transduction at a high MOI resulted in almost complete loss of viable cells, but transduction at a low MOI caused minimal growth inhibition. These results are compatible with our data in Figures 4 and 6.

We also showed that shBCR and shABL very efficiently downregulated p190/p210 Bcr-Abl proteins as well as their normal counterparts. Although Abl-deficient mice have multiple defects, including high postnatal mortality, runting and morphological abnormalities, Abl is considered to be dispensable for the function of hematopoietic stem cells, myeloid progenitor cells and immune cells.[20,21] On the other hand, Bcr-null mice appear intact, and a peculiar finding is that their neutrophils show a marked increase in superoxide production upon activation.[22] Consistent with these findings, shABL slightly inhibited proliferation of p190/p210$^-$ NALM-6 cells without loss of viability, but shBCR did not affect these cells. In addition, BaF/3-p190 cells treated with shABL and shBCR could be

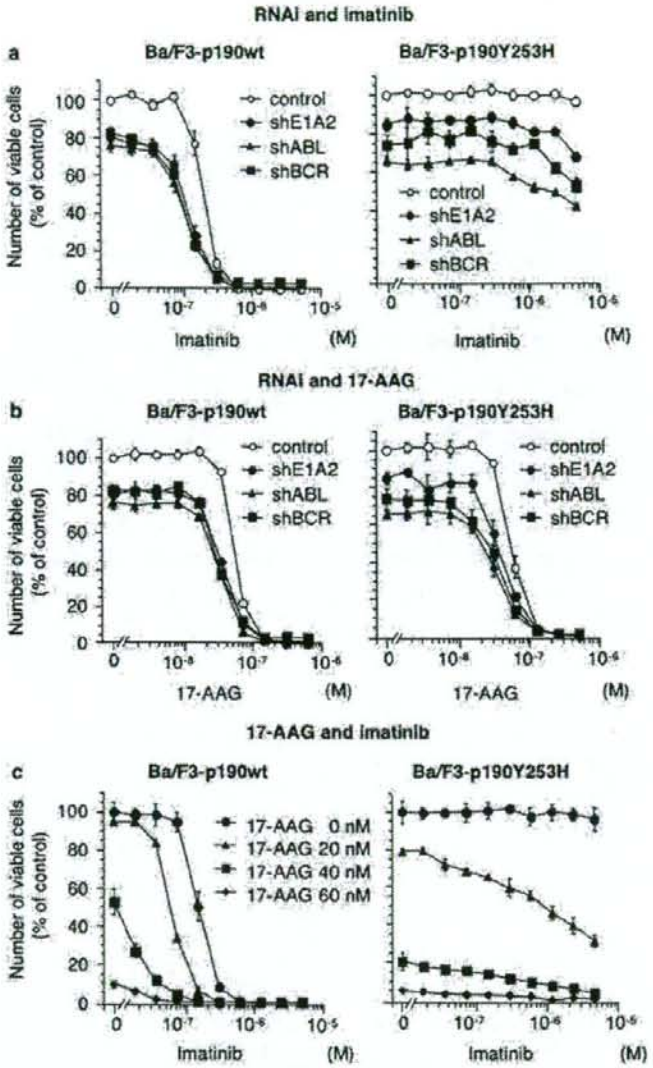

Figure 6 Cell proliferation assay conducted after combined treatment with shRNAs and imatinib or 17-AAG. (**a**) Combination of shRNAs and imatinib. Ba/F3-p190wt and Ba/F3-p190Y253H cells were transduced with shRNA lentiviral vectors under suboptimal condition (MOI = 1) and cultured in the presence or absence of imatinib (0–5 μM). (**b**) Combination of shRNAs and 17-AAG. Ba/F3-p190wt cells and Ba/F3-p190Y253H cells were transduced with shRNA lentiviral vectors at an MOI of 1 and cultured in the presence or absence of 17-AAG (0–500 nM). (**c**) Combination of 17-AAG and imatinib. Ba/F3-p190wt cells and Ba/F3-p190Y253H cells were treated with various combinations of 17-AAG (0–60 nM) and imatinib (0–5 μM). Viable cell number was determined using a WST-8 assay after the 96 h of treatment.

rescued by exogenous IL-3, indicating that neither Abl nor Bcr is essential for response to IL-3. In addition, shABL, but not shBCR, inhibited CFU-GEMM/BFU-E-derived colony formation, which suggests that Abl plays a role especially in normal erythropoiesis. Furthermore, shABL, but not shBCR, profoundly depleted 293 cells during the culture of several days, suggesting the tissue-specific critical role of Abl (data not shown). Thus, it is possible that, with an improved delivery system such as our previously developed CD19-targeted liposomes,[23] anti-p190 shRNAs may become a therapeutic option in Ph$^+$ ALL.

Hsp90 is a molecular chaperon that forms complexes with a variety of polypeptides and facilitates the initial folding and stabilization of its client proteins. Hsp90 is disrupted by 17-AAG,[24] which induces the degradation of p190/p210[18,19] and thereby inhibits the proliferation of p190/p210$^+$ cells with or without the kinase domain mutation.[25] We revealed that 17-AAG downregulated p190 and other signaling molecules downstream of p190. Some studies have shown that anti-p210 siRNA in combination with imatinib or 17-AAG exerts more potent activity than control siRNA with imatinib or 17-AAG in

p210$^+$ cells, with or without the kinase domain mutation.[12,26] In addition, Radujkovic *et al.*[27] have shown that combination treatment with 17-AAG and imatinib inhibits cell proliferation additively/antagonistically in imatinib-sensitive p210$^+$ cells and synergistically in imatinib-resistant cells. Our results are closely compatible with these data, and combination-targeting strategies, as described here, may have enhanced therapeutic potency.

The activation of Stat5 in Ph$^+$ leukemia cells is well recognized,[28,29] but its significance in the pathogenesis of Ph$^+$ leukemia is controversial. However, BCR-ABL-transduced hematopoietic progenitors from Stat5-null mice cannot generate leukemia in recipient mice,[30] and that anti-Stat5 siRNA impairs Ph$^+$ myeloid colony formation in CML.[31] These two recent studies suggest that Stat5 contributes to Bcr-Abl-induced leukemogenesis. Bcr-Abl may directly activate Stat5 through phosphorylation,[32,33] or may indirectly activate Stat5 through phosphorylation by Jak2 or Src family kinases,[28,34,35] both of which are activated in Bcr-Abl-expressing cells. Interestingly, tyrosine phosphorylation of Stat5 was substantially eliminated in BaF/3-p190wt cells transduced with anti-p190 shRNAs, whereas Jak2, Akt and MEK1/2 were still in an activated state. These results offer further evidence for the critical role of Stat5 in Bcr-Abl-induced transformation of hematopoietic cells. It is likely that p190 directly phosphorylates Stat5 and that Jak2 is remote from activation of Stat5 in this cell context, although the possible involvement of Src family kinases such as Hck and Lyn cannot be excluded. The mechanism by which phophorylation of several signal transducers was maintained after p190 down-regulation remains to be elucidated. Nevertheless, compared with the PI3K/Akt and Ras/Raf/MEK/ERK pathways, the Stat5 signaling pathway contributes more closely to p190-mediated transformation of hematopoietic cells.

In conclusion, RNAi-mediated silencing of p190 is a promising tool for both signal transduction delineation and therapeutic application in p190-expressing leukemia.

Acknowledgements

We thank Dr IM Verma (Salk Institute, La Jolla, CA, USA) and Cell Genesys for providing HIV vector constructs. We are indebted to Mr K Takahashi, Ms S Suzuki and Ms M Oiwa for technical support.

References

1 Lugo TG, Pendergast AM, Muller AJ, Witte ON. Tyrosine kinase activity and transformation potency of bcr-abl oncogene products. *Science* 1990; **247**: 1079–1082.
2 Melo JV. The diversity of BCR-ABL fusion proteins and their relationship to leukemia phenotype. *Blood* 1996; **88**: 2375–2384.
3 Druker BJ, Tamura S, Buchdunger E, Ohno S, Segal GM, Fanning S *et al.* Effects of a selective inhibitor of the Abl tyrosine kinase on the growth of Bcr-Abl positive cells. *Nat Med* 1996; **2**: 561–566.
4 Weisberg E, Manley PW, Breitenstein W, Bruggen J, Cowan-Jacob SW, Ray A *et al.* Characterization of AMN107, a selective inhibitor of native and mutant Bcr-Abl. *Cancer Cell* 2005; **7**: 129–141.
5 Lombardo LJ, Lee FY, Chen P, Norris D, Barrish JC, Behnia K *et al.* Discovery of N-(2-chloro-6-methyl- phenyl)-2-(6-(4-(2-hydroxyethyl)- piperazin-1-yl)-2-methylpyrimidin-4- ylamino)thiazole-5-carboxamide (BMS-354825), a dual Src/Abl kinase inhibitor with potent antitumor activity in preclinical assays. *J Med Chem* 2004; **47**: 6658–6661.
6 von Bubnoff N, Peschel C, Duyster J. Resistance of Philadelphia-chromosome positive leukemia towards the kinase inhibitor imatinib (STI571, Glivec): a targeted oncoprotein strikes back. *Leukemia* 2003; **17**: 829–838.
7 Deininger M, Buchdunger E, Druker BJ. The development of imatinib as a therapeutic agent for chronic myeloid leukemia. *Blood* 2005; **105**: 2640–2653.
8 Soda Y, Tani K, Bai Y, Saiki M, Chen M, Izawa K *et al.* A novel maxizyme vector targeting a bcr-abl fusion gene induced specific cell death in Philadelphia chromosome-positive acute lymphoblastic leukemia. *Blood* 2004; **104**: 356–363.
9 Elbashir SM, Harborth J, Lendeckel W, Yalcin A, Weber K, Tuschl T. Duplexes of 21-nucleotide RNAs mediate RNA interference in cultured mammalian cells. *Nature* 2001; **411**: 494–498.
10 Hannon GJ. RNA interference. *Nature* 2002; **418**: 244–251.
11 Wilda M, Fuchs U, Wossmann W, Borkhardt A. Killing of leukemic cells with a BCR/ABL fusion gene by RNA interference (RNAi). *Oncogene* 2002; **21**: 5716–5724.
12 Wohlbold L, van der Kuip H, Miething C, Vornlocher HP, Knabbe C, Duyster J *et al.* Inhibition of bcr-abl gene expression by small interfering RNA sensitizes for imatinib mesylate (STI571). *Blood* 2003; **102**: 2236–2239.
13 Li MJ, McMahon R, Snyder DS, Yee JK, Rossi JJ. Specific killing of Ph+ chronic myeloid leukemia cells by a lentiviral vector-delivered anti-bcr/abl small hairpin RNA. *Oligonucleotides* 2003; **13**: 401–409.
14 Scherr M, Battmer K, Schultheis B, Ganser A, Eder M. Stable RNA interference (RNAi) as an option for anti-bcr-abl therapy. *Gene Therapy* 2005; **12**: 12–21.
15 Wohlbold L, van der Kuip H, Moehring A, Granot G, Oren M, Vornlocher HP *et al.* All common p210 and p190 Bcr-abl variants can be targeted by RNA interference. *Leukemia* 2005; **19**: 290–292.
16 Bai Y, Soda Y, Izawa K, Tanabe T, Kang X, Tojo A *et al.* Effective transduction and stable transgene expression in human blood cells by a third-generation lentiviral vector. *Gene Therapy* 2003; **10**: 1446–1457.
17 Steelman LS, Pohnert SC, Shelton JG, Franklin RA, Bertrand FE, McCubrey JA. JAK/STAT, Raf/MEK/ERK, PI3K/Akt and BCR-ABL in cell cycle progression and leukemogenesis. *Leukemia* 2004; **18**: 189–218.
18 Nimmanapalli R, O'Bryan E, Bhalla K. Geldanamycin and its analogue 17-allylamino-17-demethoxygeldanamycin lowers Bcr-Abl levels and induces apoptosis and differentiation of Bcr-Abl-positive human leukemic blasts. *Cancer Res* 2001; **61**: 1799–1804.
19 Nimmanapalli R, O'Bryan E, Huang M, Bali P, Burnette PK, Loughran T *et al.* Molecular characterization and sensitivity of STI-571 (imatinib mesylate, Gleevec)-resistant, Bcr-Abl-positive, human acute leukemia cells to SRC kinase inhibitor PD180970 and 17-allylamino-17-demethoxygeldanamycin. *Cancer Res* 2002; **62**: 5761–5769.
20 Tybulewicz VL, Crawford CE, Jackson PK, Bronson RT, Mulligan RC. Neonatal lethality and lymphopenia in mice with a homozygous disruption of the c-abl proto-oncogene. *Cell* 1991; **65**: 1153–1163.
21 Schwartzberg PL, Stall AM, Hardin JD, Bowdish KS, Humaran T, Boast S *et al.* Mice homozygous for the ablm1 mutation show poor viability and depletion of selected B and T cell populations. *Cell* 1991; **65**: 1165–1175.
22 Voncken JW, van Schaick H, Kaartinen V, Deemer K, Coates T, Landing B *et al.* Increased neutrophil respiratory burst in bcr-null mutants. *Cell* 1995; **80**: 719–728.
23 Harata M, Soda Y, Tani K, Ooi J, Takizawa T, Chen M *et al.* CD19-targeting liposomes containing imatinib efficiently kill Philadelphia chromosome-positive acute lymphoblastic leukemia cells. *Blood* 2004; **104**: 1442–1449.
24 Prodromou C, Roe SM, O'Brien R, Ladbury JE, Piper PW, Pearl LH. Identification and structural characterization of the ATP/ADP-binding site in the Hsp90 molecular chaperone. *Cell* 1997; **90**: 65–75.
25 Gorre ME, Ellwood-Yen K, Chiosis G, Rosen N, Sawyers CL. BCR-ABL point mutants isolated from patients with imatinib mesylate-resistant chronic myeloid leukemia remain sensitive to inhibitors of the BCR-ABL chaperone heat shock protein 90. *Blood* 2002; **100**: 3041–3044.
26 Withey JM, Harvey AJ, Crompton MR. RNA interference targeting of Bcr-Abl increases chronic myeloid leukemia cell killing by 17-allylamino-17-demethoxygeldanamycin. *Leuk Res* 2006; **30**: 553–560.

27 Radujkovic A, Schad M, Topaly J, Veldwijk MR, Laufs S, Schultheis BS *et al*. Synergistic activity of imatinib and 17-AAG in imatinib-resistant CML cells overexpressing BCR-ABL–Inhibition of P-glycoprotein function by 17-AAG. *Leukemia* 2005; **19**: 1198–1206.
28 Shuai K, Halpern J, ten Hoeve J, Rao X, Sawyers CL. Constitutive activation of STAT5 by the BCR-ABL oncogene in chronic myelogenous leukemia. *Oncogene* 1996; **13**: 247–254.
29 Carlesso N, Frank DA, Griffin JD. Tyrosyl phosphorylation and DNA binding activity of signal transducers and activators of transcription (STAT) proteins in hematopoietic cell lines transformed by Bcr/Abl. *J Exp Med* 1996; **183**: 811–820.
30 Hoelbl A, Kovacic B, Kerenyi MA, Simma O, Warsch W, Cui Y *et al*. Clarifying the role of Stat5 in lymphoid development and Abelson-induced transformation. *Blood* 2006; **107**: 4898–4906.
31 Scherr M, Chaturvedi A, Battmer K, Dallmann I, Schultheis B, Ganser A *et al*. Enhanced sensitivity to inhibition of SHP2, STAT5, and Gab2 expression in chronic myeloid leukemia (CML). *Blood* 2006; **107**: 3279–3287.
32 Nieborowska-Skorska M, Wasik MA, Slupianek A, Salomoni P, Kitamura T, Calabretta B *et al*. Signal transducer and activator of transcription (STAT)5 activation by BCR/ABL is dependent on intact Src homology (SH)3 and SH2 domains of BCR/ABL and is required for leukemogenesis. *J Exp Med* 1999; **189**: 1229–1242.
33 Sillaber C, Gesbert F, Frank DA, Sattler M, Griffin sJD. STAT5 activation contributes to growth and viability in Bcr/Abl-transformed cells. *Blood* 2000; **95**: 2118–2125.
34 Wilson-Rawls J, Xie S, Liu J, Laneuville P, Arlinghaus RB. P210 Bcr-Abl interacts with the interleukin 3 receptor beta(c) subunit and constitutively induces its tyrosine phosphorylation. *Cancer Res* 1996; **56**: 3426–3430.
35 Klejman A, Schreiner SJ, Nieborowska-Skorska M, Slupianek A, Wilson M, Smithgall TE *et al*. The Src family kinase Hck couples BCR/ABL to STAT5 activation in myeloid leukemia cells. *EMBO J* 2002; **21**: 5766–5774.

Supplementary Information accompanies the paper on the Leukemia website (http://www.nature.com/leu)

Biochemical and Biophysical Research Communications 369 (2008) 801–806

Contents lists available at ScienceDirect

Biochemical and Biophysical Research Communications

journal homepage: www.elsevier.com/locate/ybbrc

Common marmoset embryonic stem cell can differentiate into cardiomyocytes

Hao Chen [a,b], Fumiyuki Hattori [a,c], Mitsushige Murata [a,b], Weizhen Li [a], Shinsuke Yuasa [a], Takeshi Onizuka [a,b], Kenichiro Shimoji [a,b], Yohei Ohno [a,b], Erika Sasaki [d], Kensuke Kimura [a,b], Daihiko Hakuno [a,b], Motoaki Sano [a], Shinji Makino [a], Satoshi Ogawa [b], Keiichi Fukuda [a,*]

[a] Department of Regenerative Medicine and Advanced Cardiac Therapeutics, Keio University School of Medicine, 35 Shinanomachi, Shinjuku-ku, Tokyo 160-8582, Japan
[b] Division of Cardiology, Department of Medicine, Keio University School of Medicine, 35 Shinanomachi, Shinjuku-ku, Tokyo 160-8582, Japan
[c] Asubio Pharma Co., Ltd., 1-1-1 Wakayamadai, Shimamoto-cho, Mishima-gun, Osaka 618–8513, Japan
[d] Laboratory of Applied Developmental Biology, Marmoset Research Department, Central Institute for Experimental Animals, 1430 Nogawa, Miyamae-ku, Kawasaki, Kanagawa 216-0001, Japan

ARTICLE INFO

Article history:
Received 7 February 2008
Available online 10 March 2008

Keywords:
Embryonic stem cell
Common marmoset
Primate
Monkey
Cardiomyocytes
Differentiation
Characterization
Heart regeneration
Preclinical model

ABSTRACT

Common marmoset monkeys have recently attracted much attention as a primate research model, and are preferred to rhesus and cynomolgus monkeys due to their small bodies, easy handling and efficient breeding. We recently reported the establishment of common marmoset embryonic stem cell (CMESC) lines that could differentiate into three germ layers. Here, we report that our CMESC can also differentiate into cardiomyocytes and investigated their characteristics. After induction, *FOG-2* was expressed, followed by *GATA4* and *Tbx20*, then *Nkx2.5* and *Tbx5*. Spontaneous beating could be detected at days 12–15. Immunofluorescent staining and ultrastructural analyses revealed that they possessed characteristics typical of functional cardiomyocytes. They showed sinus node-like action potentials, and the beating rate was augmented by isoproterenol stimulation. The BrdU incorporation assay revealed that CMESC-derived cardiomyocytes retained a high proliferative potential for up to 24 weeks. We believe that CMESC-derived cardiomyocytes will advance preclinical studies in cardiovascular regenerative medicine.

Cardiomyocytes have been known to terminally differentiate and lose their ability to proliferate soon after birth [1]. Some researchers have reported the possible existence of adult cardiac stem or progenitor cells [2–4], but unfortunately these cells do not have sufficient proliferation ability for repairing the damaged heart [5]. Therefore, once the physical or functional loss of myocytes occurs due to myocardial infarction (MI) or myocarditis, a damaged heart cannot recover its structure and function. The characteristics of embryonic stem (ES) cells include clonal and unlimited expansion, as well as differentiation into various cell types including cardiomyocytes [6]. Thus, human ES cells would be an attractive cell source for regenerative heart therapy. However, before these can be applied clinically, the therapeutic efficacy and safety of ES cell-derived cardiomyocytes must be proven in preclinical experiments using a primate model system.

To date, rhesus and cynomolgus monkeys have been the most frequently used primate models in preclinical studies. Recently, the common marmoset monkey (*Callithrix jacchus*) has attracted a great deal of attention as a potential laboratory and preclinical experimental animal, because it has many advantages including a small body, a short gestation period (approximately 144 days), early sexual maturity (12–18 months), bears 4–6 progeny/year, is cost efficient and is easy to maintain. Recently, we reported the establishment of three CMESC lines, which have many similarities to human ES cells including morphology, surface antigens and cellular characteristics [7]. It is expected that common marmoset monkeys and CMESC-derived differentiated cells will provide a powerful preclinical model for studies in the field of regenerative medicine.

Rhesus and cynomolgus monkey ES cells have already been established [8,9], and these ES cells are able to differentiate into cardiomyocytes [10,11]. We have reported previously that CMESC lines can differentiate into neuron and glia, and induce formation of teratomas including cartilage, adipose tissue, skeletal muscle, a bronchus-like structure, keratinizing squamous epidermis, epidermis and CD31-positive vascular endothelial cells [7]. However, we were not able to induce cardiomyocyte differentiation from CMESC.

To utilize this system for preclinical studies into heart regeneration, we investigated conditions that were suitable for cardiomyocyte induction from CMESC. Here we report the successful

* Corresponding author. Address: Department of Regenerative Medicine and Advanced Cardiac Therapeutics, Keio University School of Medicine, 35 Shinanomachi, Shinjuku-ku, Tokyo 160-8582, Japan. Fax: +81 3 5363 3875.
E-mail address: kfukuda@sc.itc.keio.ac.jp (K. Fukuda).

0006-291X/$ - see front matter © 2008 Elsevier Inc. All rights reserved.
doi:10.1016/j.bbrc.2008.02.141

differentiation of CMESC into cardiomyocytes. The CMESC-derived cardiomyocytes were characterized in detail.

Materials and methods

Common marmoset ES cell culture and differentiation. The CMESC lines No. 20 and 40 were obtained from the Laboratory of Applied Developmental Biology, Marmoset Research Department, Central Institute for Experimental Animals [7]. CMESCs were cultured on 10 μg/mL mitomycin C-treated mouse embryonic fibroblast (MEF) feeder cells with CMESM (common marmoset ES cell medium) culture medium, which consisted of 80% Knockout Dulbecco's modified Eagle's medium (KO-DMEM; Invitrogen Co., 10829-018) supplemented with 20% Knockout Serum Replacement® (KSR; Invitrogen Co., 10828-028), 0.1 mM MEM Non-Essential Amino Acids Solution (Sigma–Aldrich Co., M7145), 2 mM L-Glutamine (Invitrogen Co., 25030-081), 0.1 mM β-Mercaptoethanol (2-ME; Sigma–Aldrich Co., M-7522) and 4 ng/mL basic fibroblast growth factor (bFGF; Wako Pure Chemical Industries Ltd., 064-04541). CMESCs were passaged every 5 or 6 days to maintain them in an undifferentiated state.

For differentiation, CMESC colonies of an appropriate size were chosen using a combination of 40-μm and 100-μm cell-strainers (Becton–Dickinson) that also facilitated the complete removal of feeder cells. Embryoid bodies (EBs) were formed by suspending and culturing colonies in Petri dishes during the first 10 days. To evaluate the incidence of beating EBs, EBs were distributed in non-adhesive 96-well culture plates (Sumitomo Bakelite Co., Ltd.) with approximately 1–2 EBs per well.

Reverse transcription-polymerase chain reaction (RT-PCR) analysis. Total RNA was prepared from EBs using ISOGEN (Nippon gene Co., Ltd., 317-02501), according to the manufacturer's instructions. Contaminating genomic DNA was degraded by RNase-Free DNase I (Ambion, Japan, #2222) at 37 °C for 30 min. Following phenol–chloroform extraction and ethanol precipitation, total RNA was reverse transcribed into cDNA using the Oligo-(dT)12-18 primer (Superscript II RT kit; Invitrogen Co., 18064-022) and then amplified by PCR using RED-Taq DNA polymerase (Sigma–Aldrich Co., D4309). The primer sequences and PCR conditions are listed online in Supplementary Table 1.

Immunofluorescent staining. EBs (6–8 weeks after differentiation) were fixed in 4% paraformaldehyde for 30 min at room temperature, cryoprotected with sucrose and cryosectioned into 7-μm sections. After pretreatment with ImmunoBlock® (Dainippon Sumitomo Pharma Co., Ltd., KN001), the sections were incubated at 4 °C overnight with the primary antibodies diluted in TBST (Tris-buffered saline with 0.1% Tween 20). The fluorescent dye-conjugated secondary antibodies were then applied to the sections for 30 min at 37 °C. The antibodies used in this study are listed online in Supplementary Table 2. The nuclei were stained with DAPI or ToPro-3 (Invitrogen Co.) and observed by conventional fluorescent microscopy (IX71; Olympus Co.) and confocal Laser microscopy (LSM510 META; Carl Zeiss Inc.), respectively.

Transmission electron microscopy (TEM). EBs were fixed in cold 2.5% glutaraldehyde with 2% paraformaldehyde in 0.1 mol/L cacodylate buffer (pH 7.4), post-fixed in 1% osmium tetroxide, dehydrated and embedded in Epon resin. Ultrathin sections were mounted on copper grids, stained with uranyl acetate and lead citrate, and examined by TEM (Philips).

Electrophysiology. The microscope was equipped with a recording chamber and a noise-free heating plate (Microwarm Plate; Kitazato Supply). A 10 mmol/L volume of HEPES was added to the culture medium to maintain the pH of the perfusate at 7.5–7.6. Standard glass microelectrodes that had a DC resistance of 25–35 MΩ when filled with pipette solution (2 mol/L KCl) were used. The electrodes were positioned using a motor-driven micromanipulator (EMM-3SV; Narishige) under optical control. Spontaneously beating cells were selected as targets, and the action potentials of the targeted cells were recorded. The recording pipette was connected to a patch-clamp amplifier (Axopatch 200B; Axon Instruments), and the signal was passed through a low-pass filter with a cut-off frequency of 2 kHz and digitized with an A/D converter with a sampling frequency of 10 kHz (Digidata 1440A; Axon Instruments). Signals were monitored, recorded as electronic files, and analyzed offline with pCLAMP 10 software (Axon Instruments).

BrdU incorporation assay. After three weeks of differentiation, the medium was changed and EBs were cultured in α-MEM supplemented with 10% FCS. Five to 36-week-old EBs were divided into two groups. EBs in Group 1 (intact EB) were cultured with 10 μmol/L of BrdU for 24 h in α-MEM supplemented with 10% FCS, then fixed with 4% paraformaldehyde. After treatment with 20% sucrose for 1 hour at RT, the fixed cells were cryosectioned. The sections were immersed in 2 N HCl with 0.5% Tween 20 solution for 20 min. Cardiomyocytes that had incorporated BrdU were detected using the BrdU Labeling and Detection Kit I (Roche Diagnostics Co., 11296736001) according to the manufacturer's instructions, except that the primary antibody for Nkx2.5 and the secondary antibody conjugated with Alexa-546 (Invitrogen Co.) were also used to identify cardiomyocytes. EBs in Group 2 (dispersed condition) were dispersed by 0.1% trypsin and 0.1% collagenase type III (Worthington Biochemical Co., #4182) in ADS buffer (116 mM NaCl, 20 mM HEPES, 12.5 mM NaH_2PO_4, 5.6 mM glucose, 5.4 mM KCl, and 0.8 mM $MgSO_4$, pH 7.35) with stirring. After 2 days of culture in α-MEM supplemented with 10% FCS, 10 μmol/L of BrdU was added and the dispersed EBs were cultured for a further 24 h at 37 °C in the same medium. Detection of BrdU-incorporated cardiomyocytes was performed as described above.

Results

Differentiation of CMESCs into spontaneously contracting cardiomyocytes

The two lines of CMESCs were cultured in medium containing KSR instead of animal-derived serum in order to maintain pluripotency (Fig. 1A, left). To stimulate the CMESCs to differentiate into cardiomyocytes, we adopted a conventional floating culture system and tested several combinations of medium (DMEM, KO-DMEM or α-MEM) and several lots of fetal calf serum (FCS) or KSR. We succeeded in stimulating CMESC line No. 20 to differentiate into contracting EBs, but failed to differentiate CMESC line No.40 under all conditions tested. CMESC line No. 20 could differentiate into EBs with contracting areas when a combination of three out of five lots of FCS (5–20% in use) and KO-DMEM or α-MEM were used. Strikingly, beating EBs could be obtained very efficiently by culturing the cells in KO-DMEM supplemented with 20% KSR, which was named dCMESM (common marmoset ES cell medium for cardiomyocyte differentiation). This had the same composition as the CMESM, but lacked bFGF. Confluent cultures of undifferentiated CMESCs were completely dissociated from the feeder cells and cultured in suspension to form EBs in dCMESM. In the floating culture system, CMESCs efficiently developed EBs and spontaneously beating cells (Supplementary Movie). An average of 10–20% of EBs began spontaneously contracting 12–15 days after differentiation. A maximum percentage (46 ± 13%) of contractile EBs was observed at approximately 18 days after differentiation, and was roughly sustained for two months.

Most contractile areas within EBs were located in the cell mass or the periphery of cystic structures. Contraction of CMESC-derived EBs was highly sensitive to temperature, a characteristic shared by human ES-derived EBs. EBs were cryosectioned 6–8 weeks after differentiation and immunofluorescent staining was performed. Typically Nkx2.5 and α-Actinin double-positive areas existed in the subsurface of EBs (Fig. 1A, center and right). In the cardiomyocyte-containing EBs, the Nkx2.5 and α-Actinin double-positive cells were approximately 30% of total cells.

Immunofluorescent staining and microstructure of CMESC-derived cardiomyocytes

Immunofluorescent staining was essential to determine the cardiomyocyte structure and the expression of cardiomyocyte-specific proteins. However, at the start of this study, the type of antibodies that would recognize common marmoset monkey cardiomyocytes was unknown. We therefore tested various antibodies that could detect cardiomyocyte-specific proteins in the CMESC-derived cardiomyocytes. Spontaneously beating EBs were dispersed and the CMESC-derived cardiomyocytes were cultured under adherent culture conditions. Immunofluorescent staining was then performed. Antibodies for the cardiac-specific transcription factors Nkx2.5 and GATA4 strongly labeled the nuclei of the CMESC-derived cardiomyocytes. Moreover, antibodies for α-Actinin, myosin heavy chain (MHC), myosin light chain (MLC) and Tropomyosin strongly labeled the typical myofilament structure of the cardiomyocytes. The antibody for the atrial natriuretic peptide (ANP) highlighted the secretary granules typical of cardiomyocytes surrounding the nucleus (Fig. 1B).

Microstructural analysis using TEM revealed typical myofilament structures, desmosomes and a number of mitochondria in CMESC-derived cardiomyocytes (Fig. 1C).

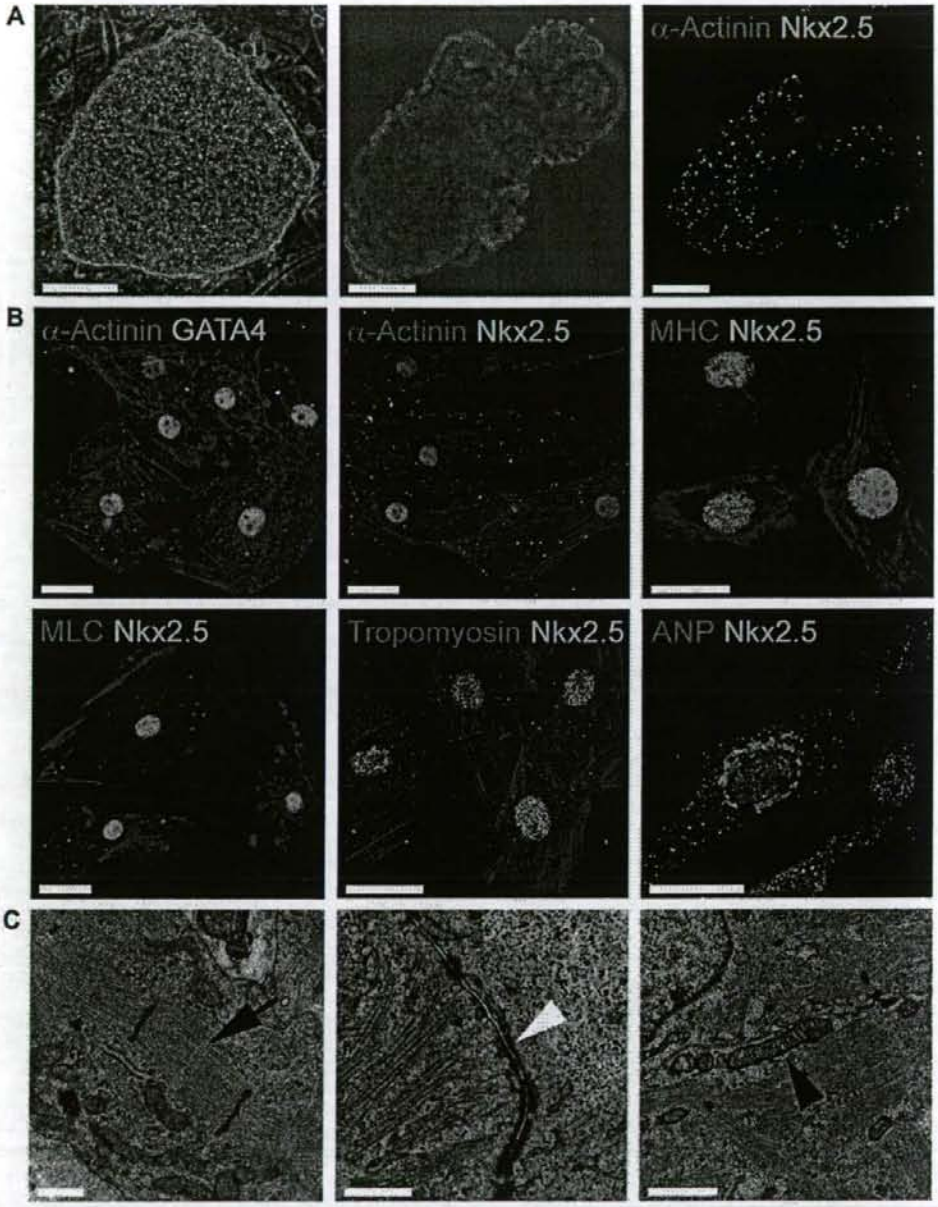

Fig. 1. Structural studies of CMESC-derived cardiomyocytes. (A) Phase contrast microscopy of the undifferentiated CMESC (left), and typical cardiomyocyte-containing non-cystic embryoid body (EB) (center). Immunofluorescent microscopy of cryosections of EBs using anti-α-Actinin and Nkx2.5 antibodies. (B) Double immunofluorescent staining for Nkx2.5 or GATA4 combined with α–Actinin, MHC, MLC, Tropomyosin or ANP. (C) Transmission electron microscopy of the CMESC-derived cardiomyocytes: striated muscle fiber (left, black arrow), desmosomal structure (middle, white arrow head) and mitochondria (right, black arrow head). Scale bars: (A) 100 μm; (B), 20 μm; (C) 0.5 μm.

Time course of marker gene expression during cardiomyocyte differentiation

To characterize the differentiation pathway of undifferentiated CMESC into cardiomyocytes, we performed semi-quantitative RT-PCR to analyze the expression of various marker genes associated with pluripotency, visceral endoderm, and early and late cardiomyogenesis. Some of the primers used have been described previously [7,10], and some were designed based on similar murine, *macaca fascicularis* and *homo sapiens* sequences (Supplementary Table 1). The pluripotency markers *Nanog* and octamer-binding transcription factor 3 (*Oct3/4*) were expressed at high levels in

undifferentiated ES cells. Expression levels of both markers gradually decreased upon differentiation and completely disappeared at day 15 post-differentiation (Fig. 2A). The early mesendoderm marker *Brachyury* was observed from day 3 post-differentiation, peaked at day 6 post-differentiation, but could not be detected at day 9 post-differentiation (Fig. 2B). The visceral endoderm marker alpha-fetoprotein (*AFP*) was observed from day 3 post-differentiation and peaked at day 9 post-differentiation, but could not be detected at day 15 post-differentiation (Fig. 2C). For the genes encoding cardiac-related transcription factors, the expression of the friend of GATA 2 (*FOG-2*) was first observed from day 3 post-differentiation, *GATA4* and the t-box 20 (*Tbx-20*) were from day 6 post-differentiation, *Tbx5* was from day 9 post-differentiation, and *Nkx2.5* was strongly observed at day 15 post-differentiation (Fig. 2D). For the cardiomyocyte-specific proteins, *ANP* and the MLC 2 atrial (*MLC2a*) were observed first from day 6 post-differentiation, *α-MHC* and *β-MHC* were from day 9 post-differentiation, the MLC 2 ventricular (*MLC2v*) was from day 12 post-differentiation (Fig. 2E).

Action potential recordings of CMESC-derived cardiomyocytes

We recorded the action potentials of CMESC-derived cardiomyocytes using glass microelectrodes. Eight-week-old contracting EBs were selected manually and dispersed into small clumps and single cells. The dispersed EBs were cultured to confluence for three days before analysis. The microelectrode was advanced to the intracellular cytoplasm and the voltage of the bulk solution and cytoplasm were measured. Rhythmic beating could be detected in the CMESC-derived cardiomyocytes. The action potential resembled a sinus node, indicating that the CMESC-derived cardiomyocytes had a relatively shallow resting membrane potential, slow diastolic depolarization and relatively long action potential duration (Fig. 3A). The administration of isoproterenol increased their beating rates (Fig. 3B). The basic cycle length (BCL), action potential duration (APD), d*V*/d*t*, action potential amplitude (APA) and maximum diastolic potential (MDP) were also recorded (Fig. 3C).

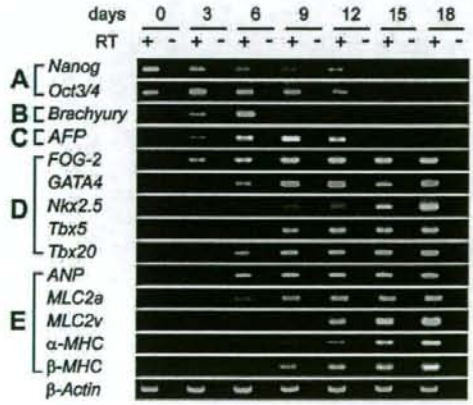

Fig. 2. RT-PCR analysis of the CMESC-derived EBs for various immature and cardiomyocyte-specific proteins. (A) Pluripotency-related genes: *Nanog* and *Oct3/4*; (B) Mesodermal marker gene: *Brachyury*; (C) Primitive endodermal marker gene: *AFP*; (D) cardiomyocyte-precursor and cardiomyocyte marker genes: *FOG-2*, *GATA4*, *Nkx2.5*, *Tbx5*, and *Tbx20*; (E) Cardiomyocyte-associated structural protein genes: *ANP*, *MLC2a*, *MLC2v*, *α-MHC*, *β-MHC*, and equal loading control β-actin. Reverse-transcription negative controls were also amplified and loaded in the lane next to the relevant sample. Abbreviations are listed in Supplementary Table 1.

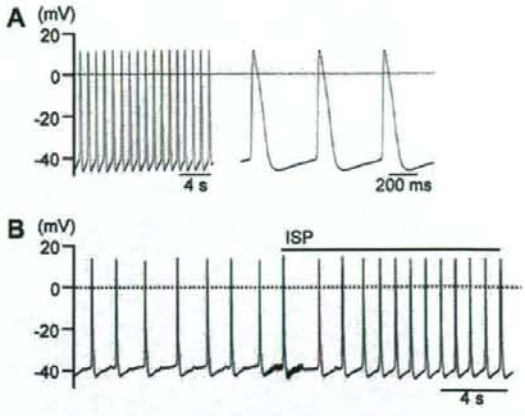

C

BCL (sec)	APD50 (msec)	APD90 (msec)
1.3~3.2	178.1±4.2	316.6±5.8

dV/dt max (V/s)	APA (mV)	MDP (mV)	n
5.6±1.0	68.4±2.5	-45.4±1.8	12

Fig. 3. Electrophysiology of CMESC-derived cardiomyocytes. (A) Representative action potentials of CMESC-derived cardiomyocytes showing spontaneous beating (left) and the relatively short duration time of the action potential (right). (B) Effect of isoproterenol (ISP) on the beating rate. (C) Statistical parameters obtained from 12 cardiomyocytes including beating cycle length (BCL), action potential duration (APD), d*V*/d*t* max, action potential amplitude (APA) and maximum diastolic potential (MDP).

Proliferative potential of CMESC-derived cardiomyocytes

Since the gestation period of the common marmoset is approximately seven times longer than that of the mouse, we hypothesized that CMESC-derived cardiomyocytes also retain their proliferative potential for a longer period of time and investigated this possibility. When EBs were dispersed into small clumps we observed a relatively long-term proliferation period and noticeable cell multiplication. From these findings, we expected that CMESC-derived cardiomyocytes might possess a higher proliferation ability than mouse-derived ES cells.

First, we performed BrdU incorporation assays on intact EBs at several time points after differentiation had occurred. The identification of DNA synthesizing cardiomyocytes was confirmed by co-immunofluorescent staining of Nkx2.5 and BrdU. At 6 weeks, intact EBs initially contained 33% BrdU-positive cardiomyocytes, but this decreased to less than 1% at 12 weeks (Fig. 4A and B). Next, the dispersed cells from EBs at several time points were applied to BrdU incorporation assays. Average 73% of cardiomyocytes were positive for BrdU at 5 weeks. This gradually decreased to 30% at 24 weeks, and 0% at 36 weeks (Fig. 4A and C). Most of the cardiomyocytes from freshly dispersed EBs 36 weeks after differentiation were rod-shaped (data not shown). These data indicated that common marmoset ES cell-derived cardiomyocytes retained their proliferation potential for an extended period of time.

Discussion

This is the first study to demonstrate that CMESC can differentiate into cardiomyocytes *in vitro*. We described their overall differentiation mechanism including time-courses for the expression of various genes during cardiogenesis, and characterized them in

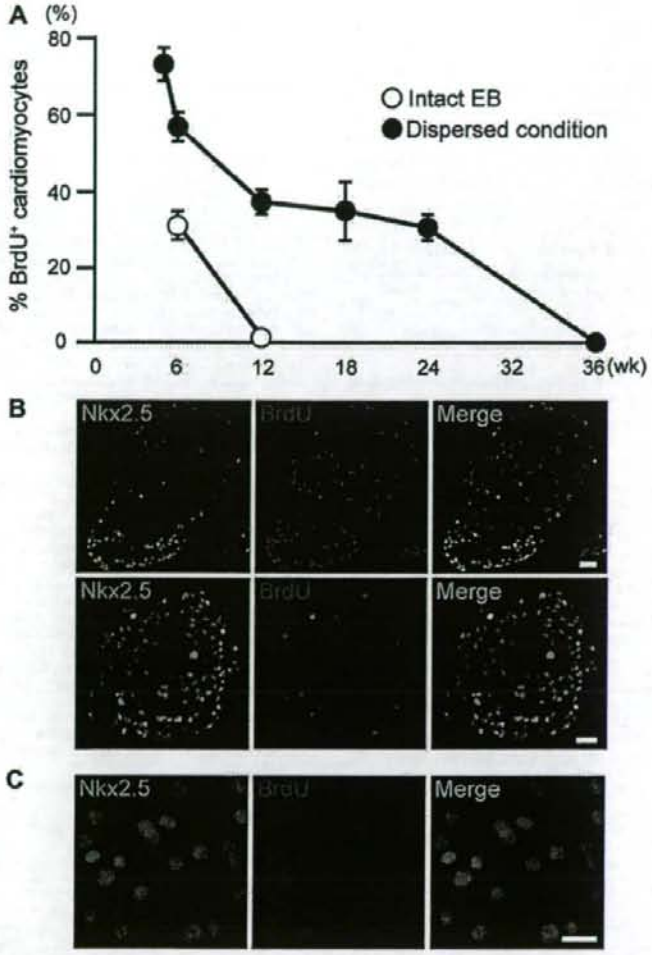

Fig. 4. Proliferation properties of CMESC-derived cardiomyocytes. (A) Time course BrdU incorporation assay in intact EB (open circle; $n = 3$) and dispersed condition (closed circle; $n = 3$) during weeks 5–36 post-differentiation. Cardiomyocytes were identified by immunofluorescent staining for Nkx2.5. The fractions of BrdU-positive cardiomyocytes were plotted. (B) Typical immunofluorescent staining patterns of Nkx2.5 (left), BrdU (middle) and merged images (right) in the intact EBs 6 weeks after differentiation (upper panel) and 12 weeks after differentiation (lower panel). (C) Typical immunodetection of Nkx2.5 (left), BrdU (middle) and merged images (right) in the dispersed condition 6 weeks after differentiation. Scale bars: (B) 100 μm; (C) 20 μm.

detail by immunofluorescent staining, ultrastructural analysis, electrophysiology and determining their growth properties.

Gene expression analyses during cardiogenesis in several species including mice [12], humans [13], and rhesus monkeys [10] are available. The present study enabled us to obtain gene expression data for the common marmoset monkey. A comparison of gene expression profiles between the species listed above highlights many similarities. The only major difference seems be in the timing of cardiomyocyte development: 8–14 days in humans; 12 days in the common marmoset; 8 days in the rhesus monkey; and 6 days in mice. Although minor differences in the expression timings of the *ANP*, *MLC-2a*, *MLC-2v* and *α-MHC* genes also exist during differentiation, we found that the timing of CMESCs was closest to human ES cells.

We found that the efficiency of cardiac differentiation was the same when obtained under non-serum conditions using KSR instead of FCS. These observations indicated that CMESCs, unlike human [14] or rhesus monkey [10] ES cells, do not require any serum-derived stimulating factors for mesendoderm induction and cardiogenesis, because KSR does not contain any cytokines or growth factors. On the other hand, the expression of various marker genes during cardiogenesis was very similar to that seen in human [14] and rhesus monkey [10] ES cells, suggesting that CMESCs have a similar cardiogenic differentiation system to human and rhesus monkey ES cells. CMESCs might be able to provide differentiation-inducing auto- and/or paracrine factors. Further mechanistic comparative studies between CMESCs and human and/or rhesus monkey ES cells will provide further insights into cardiogenic differentiation.

BrdU incorporation assay indicated that CMESC-derived cardiomyocytes were capable of long-term proliferation for extended periods of time. Importantly, CMESC-derived cardiomyocytes were still able to proliferate 24 weeks after differentiation, but the ability to proliferate ended at 36 weeks. Considering the gestation

period of the common marmoset, these findings had a reasonable explanation.

Much information about human ES cells and their application to heart regeneration therapy has accumulated [15,16]. Moreover, mouse and human inducible pluripotent stem cells (iPS cell) have also been established [17]. In order for heart regeneration therapy using regenerated cardiomyocytes to become a reality, preclinical studies using primate ES cell- or iPS cell-derived cardiomyocytes for transplantation are necessary. The common marmoset monkey is an ideal primate model for preclinical studies in the field of regenerative medicine. We believe that this report provides fundamental details about CMESC-derived cardiomyocytes that will aid their use as a primate heart cell-therapy model.

Appendix A. Supplementary data

Supplementary data associated with this article can be found, in the online version, at doi:10.1016/j.bbrc.2008.02.141.

References

[1] W.R. MacLellan, M.D. Schneider, Genetic dissection of cardiac growth control pathways, Annu. Rev. Physiol. 62 (2000) 289–319.
[2] B. Dawn, A.B. Stein, K. Urbanek, M. Rota, B. Whang, R. Rastaldo, D. Torella, X.L. Tang, A. Rezazadeh, J. Kajstura, A. Leri, G. Hunt, J. Varma, S.D. Prabhu, P. Anversa, R. Bolli, Cardiac stem cells delivered intravascularly traverse the vessel barrier, regenerate infarcted myocardium, and improve cardiac function, Proc. Natl. Acad. Sci. USA 102 (2005) 3766–3771.
[3] K.L. Laugwitz, A. Moretti, J. Lam, P. Gruber, Y. Chen, S. Woodard, L.Z. Lin, C.L. Cai, M.M. Lu, M. Reth, O. Platoshyn, J.X. Yuan, S. Evans, K.R. Chien, Postnatal isl1+ cardioblasts enter fully differentiated cardiomyocyte lineages, Nature 433 (2005) 647–653.
[4] H. Oh, S.B. Bradfute, T.D. Gallardo, T. Nakamura, V. Gaussin, Y. Mishina, J. Pocius, L.H. Michael, R.R. Behringer, D.J. Garry, M.L. Entman, M.D. Schneider, Cardiac progenitor cells from adult myocardium: homing, differentiation, and fusion after infarction, Proc. Natl. Acad. Sci. USA 100 (2003) 12313–12318.
[5] S. Lyngbaek, M. Schneider, J.L. Hansen, S.P. Sheikh, Cardiac regeneration by resident stem and progenitor cells in the adult heart, Basic Res. Cardiol. 102 (2007) 101–114.
[6] I. Kehat, D. Kenyagin-Karsenti, M. Snir, H. Segev, M. Amit, A. Gepstein, E. Livne, O. Binah, J. Itskovitz-Eldor, L. Gepstein, Human embryonic stem cells can differentiate into myocytes with structural and functional properties of cardiomyocytes, J. Clin. Invest. 108 (2001) 407–414.
[7] E. Sasaki, K. Hanazawa, R. Kurita, A. Akatsuka, T. Yoshizaki, H. Ishii, Y. Tanioka, Y. Ohnishi, H. Suemizu, A. Sugawara, N. Tamaoki, K. Izawa, Y. Nakazaki, H. Hamada, H. Suemori, S. Asano, N. Nakatsuji, H. Okano, K. Tani, Establishment of novel embryonic stem cell lines derived from the common marmoset (Callithrix jacchus), Stem Cells 23 (2005) 1304–1313.
[8] J.A. Thomson, J. Kalishman, T.G. Golos, M. Durning, C.P. Harris, R.A. Becker, J.P. Hearn, Isolation of a primate embryonic stem cell line, Proc. Natl. Acad. Sci. USA 92 (1995) 7844–7848.
[9] H. Suemori, T. Tada, R. Torii, Y. Hosoi, K. Kobayashi, H. Imahie, Y. Kondo, A. Iritani, N. Nakatsuji, Establishment of embryonic stem cell lines from cynomolgus monkey blastocysts produced by IVF or ICSI, Dev. Dyn. 222 (2001) 273–279.
[10] K. Schwanke, S. Wunderlich, M. Reppel, M.E. Winkler, M. Matzkies, S. Groos, J. Itskovitz-Eldor, A.R. Simon, J. Hescheler, A. Haverich, U. Martin, Generation and characterization of functional cardiomyocytes from rhesus monkey embryonic stem cells, Stem Cells 24 (2006) 1423–1432.
[11] M. Hosseinkhani, K. Hasegawa, K. Ono, T. Kawamura, T. Takaya, T. Morimoto, H. Wada, A. Shimatsu, S.G. Prat, H. Suemori, N. Nakatsuji, T. Kita, Trichostatin A induces myocardial differentiation of monkey ES cells, Biochem. Biophys. Res. Commun. 356 (2007) 386–391.
[12] K.R. Boheler, J. Czyz, D. Tweedie, H.T. Yang, S.V. Anisimov, A.M. Wobus, Differentiation of pluripotent embryonic stem cells into cardiomyocytes, Circ. Res. 91 (2002) 189–201.
[13] A. Beqqali, J. Kloots, D. Ward-van Oostwaard, C. Mummery, R. Passier, Genome-wide transcriptional profiling of human embryonic stem cells differentiating to cardiomyocytes, Stem Cells 24 (2006) 1956–1967.
[14] E. Bettiol, L. Sartiani, L. Chicha, K.H. Krause, E. Cerbai, M.E. Jaconi, Fetal bovine serum enables cardiac differentiation of human embryonic stem cells, Differentiation 75 (2007) 669–681.
[15] O. Caspi, I. Huber, I. Kehat, M. Habib, G. Arbel, A. Gepstein, L. Yankelson, D. Aronson, R. Beyar, L. Gepstein, Transplantation of human embryonic stem cell-derived cardiomyocytes improves myocardial performance in infarcted rat hearts, J. Am. Coll. Cardiol. 50 (2007) 1884–1893.
[16] M.A. Laflamme, K.Y. Chen, A.V. Naumova, V. Muskheli, J.A. Fugate, S.K. Dupras, H. Reinecke, C. Xu, M. Hassanipour, S. Police, C. O'Sullivan, L. Collins, Y. Chen, E. Minami, E.A. Gill, S. Ueno, C. Yuan, J. Gold, C.E. Murry, Cardiomyocytes derived from human embryonic stem cells in pro-survival factors enhance function of infarcted rat hearts, Nat. Biotechnol. 25 (2007) 1015–1024.
[17] K. Takahashi, S. Yamanaka, Induction of pluripotent stem cells from mouse embryonic and adult fibroblast cultures by defined factors, Cell 126 (2006) 663–676.